Pre-metabolic syndrome transcriptional response of adipose tissue and liver to obesity in the Ossabaw pig model

Catarina Ventura
Technical University of Denmark
Buwen Liang
Center for non-coding RNA in Technology and Health
Katharina B. Kuentzel
University of Copenhagen
Jan Gorodkin
Center for non-coding RNA in Technology and Health
Trisha J. Grevengoed
University of Copenhagen
Peter M. H. Heegaard
pmhh@dtu.dk

Technical University of Denmark

Research Article

Keywords: Ossabaw pig obesity model, RNA seq transcriptomics, transcriptional response to obesity

Posted Date: December 6th, 2025

DOI: https://doi.org/10.21203/rs.3.rs-8039124/v1

Additional Declarations: No competing interests reported.

Abstract

Background

The global rise in obesity prevalence highlights an urgent need to understand its underlying pathophysiology, which ranges from preclinical obesity (excess body fat without overt disease) to clinical obesity with impairment of organ function. To study obesity, we fed obesity-prone Ossabaw pigs a medium cholesterol (0.5 weight %), high-fat (50% of energy) and high-fructose (21% of energy) diet (MC-HFD) for relatively short-term (11 weeks). Morphometric parameters, adipocyte area, and blood biomarkers of metabolic syndrome and inflammation were evaluated. Furthermore, RNA sequencing was adopted to characterize the transcriptome-wide response to this obesogenic challenge and identify key genes and molecular processes affected by the attained obesity state in visceral adipose tissue (VAT) and liver.

Results

Pigs fed the MC-HFD diet exhibited significant increases in body weight, body size, and adipocyte area compared to the control group. However, these pigs remained metabolically healthy, with only a minor increase in low-density lipoprotein (LDL), and normal C-reactive protein, triglyceride, glucose, and insulin levels. In VAT, 666 differentially expressed transcripts (DETs) were identified, while only 40 were found in liver tissue. Notably, FASN was the only transcript that was regulated similarly (significantly downregulated) in both tissues of MC-HFD pigs, suggesting tissue-specific transcriptional signatures.

In VAT, transcripts related to the mitochondrial respiratory chain complex, protein synthesis, spliceosome and certain extracellular matrix components were upregulated, while collagen, GPCR signalling and fatty acid metabolism were generally downregulated. Compared to VAT, the liver of MC-HFD fed pigs exhibited a greater enrichment in transcripts commonly linked to obesity. Transcripts related to fatty acid biosynthesis and amino acid catabolism were suppressed, while hormone and lipoprotein metabolism associated transcripts were upregulated.

Conclusions

Taken together the data presented here suggest that MC-HFD fed Ossabaw pigs attained a pre-metabolic syndrome state of obesity characterized by an ‘obesity tolerant’ transcriptional response in VAT in contrast to the liver response resembling an early canonical obesity response.

Background

According to the World Health Organization (WHO), 16% of adults, about 1 in 8 people, were living with obesity in 2022[1]. This prevalence is expected to rise by more than 115% between 2010 and 2030[2]. As a central component of metabolic syndrome (MetS), which constitutes a major risk factor for non-communicable diseases, obesity contributes to millions of premature deaths each year, representing a serious and growing threat to global health[2]. Despite the increased burden of obesity, there are still significant gaps in our understanding of its causes and pathophysiology. The Lancet commission, in early 2025, agreed that disruptions in the biological mechanisms regulating fat mass, its distribution and function are central to the problem, however, the factors underlying these alterations are still not fully understood[3]. There is a need for research to elucidate the genetic and environmental mechanisms driving obesity and its progression into clinical obesity[3]. Investigating how environmental factors influence gene expression profiles in metabolically relevant tissues can provide key insights into the molecular mechanisms involved in obesity. To accomplish this, animal models mimicking the human obesity state and its related metabolic complications are crucial. Pigs are regarded as superior models for obesity with highly increased translational validity compared to rodent models[4]. In particular, the Ossabaw pig has been described as an outstanding model for human obesity, accurately reproducing the most complete MetS of all investigated pig breeds [5].

The WHO defines obesity as an excessive accumulation of body-fat commonly measured by body mass index (BMI)[1]. While this measure is useful at the population level, it lacks accuracy in determining individual health status. Therefore, it is recommended to also include a direct measure of body fat, yet, when this is not available, an appropriate anthropometric measure such as waist circumference should be used[3]. In pigs there is no generally accepted adiposity index, however, Dyson et al. (2006)[6] suggest the use of abdominal circumference (ABC) as an indirect measure of visceral fat in Ossabaw pigs. Excess adiposity can directly affect the structure and function of several tissues and organs, including adipose tissue (AT), liver, and heart. Specifically, AT is an important energy reservoir but also a dynamic endocrine organ playing a central role in metabolic regulation. In obesity, adipocytes undergo hypertrophy, which can contribute to changes in lipid metabolism, insulin sensitivity and inflammation[7]. While visceral AT (VAT) is more metabolically active with a stronger influence on health outcomes, subcutaneous AT (SAT) primarily functions as a storage compartment[8]. The liver plays a central role in lipid and glucose metabolism, and both obesity and MetS are associated with disruptions in these processes[9]. The heart is also impacted by obesity, particularly through the dysregulation of cardiac fatty acid metabolism[10].

RNA sequencing offers a comprehensive, untargeted method for identifying transcriptional changes in response to an experimental condition, making it a powerful tool for uncovering key biological pathways involved in obesity development[11].

Extensive work has investigated diet-induced obesity and associated comorbidities in porcine models. However, most studies focus on establishing a metabolically unhealthy phenotype[12–16]. This leaves a critical gap in our understanding of the early phases of obesity. During the early phases of obesity, the timing and extent of initial mechanisms responsible for metabolic disturbances and subsequent dysfunction may be studied in various tissues, as a deeper understanding of these mechanisms requires data obtained at multi-tissue level. For example, in mice subjected to high-fat overfeeding, insulin resistance first appears in the liver around week 6, followed by AT by week 12, while skeletal muscle retains insulin sensitivity[17].

To this end, RNA sequencing was performed on SAT, VAT, heart, and liver to analyse transcriptional differences between pigs fed a high-fat, high-fructose diet with 0.5% (medium concentration) cholesterol (MC-HFD) and those on a chow diet (control) for 11 weeks. Transcript level analysis has the advantage of capturing isoform-specific expression changes that remain undetectable at the gene level. Following aggregation of differential transcript expression data to gene level, we conducted enrichment and network analysis to elucidate the functional significance of the observed changes, offering new hypotheses that may help clarify the molecular profile in this model of obesity. We found that although pigs fed the MC-HFD diet developed obesity morphometrically, they did not exhibit a full metabolic syndrome. This pre-metabolic syndrome obese state was associated with a distinct transcriptional response in VAT, differing from the typical inflammatory and glycolytic profiles usually linked to obesity and metabolic syndrome. In contrast, the liver response resembled an early canonical obesity signature.

Materials and Methods

Study approvals, animals and housing

The study was approved by the Danish Animal Experiments Inspectorate (permit 2016-15-0201-01022) and complies with the ARRIVE guidelines. The experimental procedures were performed in accordance with Danish laws and regulations regarding the use of animals in research (The Danish Ministry of Justice, Act on Animal Experiments no. 474 of 15 May 2014, as stipulated in the executive order no. 12 on 7 January 2016), and all animal handling complied with DTU's Animal Welfare Policy. All animals were obtained from the Ossabaw facility at the Technical University of Denmark (https://ossabaw.dtu.dk) and housed at the University of Copenhagen animal facility. The experiments were specifically approved by the institutional animal ethics committee at University of Copenhagen as project number P 19–409.

The pigs were kept in a temperature-controlled environment (20–22°C) with a natural light cycle and *ad libitum* access to water. Straw bedding and enrichment was available. The study used fifteen (based on statistical power calculation) male, castrated miniature Ossabaw pigs aged 6.1 ± 1.1 (mean±SD, min = 5, max = 8) months.

Diet intervention

The animals were randomized into two groups: a control group fed a standard chow diet (control, n = 6) (SDS Diets, 3.3 kcal/g) and a group fed a customized obesogenic diet (4.6 kcal/g, custom-made at Foulum, Aarhus University, Denmark), as previously described[18], containing high-fat (48% energy), high-fructose (21% energy), and 0.5% cholesterol (MC-HFD, n = 9). A period of four weeks was used to gradually transition the pigs from normal to the MC-HFD feed. See Fig. 1 for the experimental setup and supplementary Table S1 for details concerning the diets. The control group was fed restricted chow diet according to the scheme by Swindle and Smith (2015)[19], i.e. with a daily allowance restricted to approximately 2.5% of the body weight, but not surpassing 900 g/pig/day, while the MC-HFD group was fed a fixed amount of 1 kg/pig/day. Fasting blood samples, collected in uncoated tubes (for serum preparation), were obtained, and body weight (BW), length from snout to base of tail and abdominal circumference (ABC) at the umbilicus was recorded for all pigs once weekly throughout the study. Prior to blood collection the animals were sedated by intramuscular injection of Zoletil (1 ml/10 kg, Virbac). After 11 weeks of full MC-HFD feeding, the animals were sedated as described above and then euthanized by intracardiac injection of pentobarbital (0.25 mL/kg bodyweight, sodium pentobarbital, 400 mg/mL, Euthanimal (Alfasan)). In diet week 2, the pigs were affected by a bacterial infection (gastrointestinal) and therefore received antibiotics.

Sampling and storage

At necropsy, abdominal SAT, mesenteric VAT, liver and heart were collected in RNAlater (Invitrogen), as well as in formalin and flash frozen in liquid nitrogen, and blood samples were obtained for serum preparation. RNAlater tubes were stored at room temperature overnight and subsequently stored at -20°C prior to RNA extraction. Formalin tubes were stored at 4°C. Flash frozen samples in cryogenic tubes were immediately stored at -80°C. Uncoated blood sampling tubes were stored overnight at 4°C prior to serum preparation on the next day by centrifugation (10 min, 3000 rpm)[20].

Morphometric measures

Abdominal circumference and length latest measurements were performed at week 10. BMI was calculated as in humans, as BW in kg divided by the square of body length[21]. Body surface area (BSA) was estimated using a formula suggested for miniature swine[22]: $BSA = 0.121BW^{0.575}$.

Histology and area quantification of adipocytes

Both VAT and SAT samples from MC-HFD and control pigs were fixed in 10% neutral-buffered formalin, paraffin embedded, sectioned at 3 µm and mounted on SuperFrost Plus Microscope slides (Menzel-Glaser, Braunschweig, Germany). Sections were stained with hematoxylin for 13 sec followed by rinsing in running tap water. The stained sections were imaged using the 20X objective in the Pannoramic Midi II digital slide scanner (3DHISTECH Ltd., Budapest, Hungary). Images were viewed with the slideViewer software v.2.8 also from 3DHISTECH and 10X images were exported. Adipocyte area was quantified, blinded to diet group, using ImageJ and the AdipoQ plugin[23]. Briefly, custom preferences for AdipoQ Preparator and AdipoQ were used to identify and analyse adipocytes. Several adipocyte area data points were excluded due to large portion of damaged/broken cells and/or poor segmentation.

Biochemistry and biomarker profile in serum samples

Triglycerides, fructosamine (a marker of medium-term glucose control in pigs[24]), total cholesterol, high-density lipoprotein (HDL), low-density lipoprotein (LDL) and liver enzymes were measured by an external laboratory (see acknowledgments). For these, only data from week − 3 was available to represent the start of the experiment. Glucose serum concentration was determined by a blood glucose meter (Accu-check, No. 225702) according to the manufacturer's instructions. Insulin concentration was quantified by Porcine Insulin ELISA kit (Mercodia, No. 10-1200-01) according to the manufacturer's protocol. The detection limit of 2.81 mU/L (19.49 pM) was used when the optical density (OD) was below the standard curve minimum OD. C-reactive protein (CRP) concentration was measured by a sandwich in-house ELISA as described previously[25]. The limit of detection of 4.26 mg/l was used when the OD was below the minimum OD of the standard curve. ELISA measurements were performed in duplicate for each sample and only mean values with a coefficient of variation below 15% were included in the analysis. Pig specific ELISAs for leptin and adiponectin were from My Biosource (No. MBS703419) and Assay Genie (No. PRFI00006), with the limit of detection of 0.26 ng/l and 3.125 µg/ml, respectively.

RNA extraction and sequencing

As pigs no. 1 (control) and no. 30 (MC-HFD group) showed unusual weight trajectories (Fig, 1S) they were excluded from the sample set subjected to RNA sequencing.

Total RNA was extracted from liver, heart, SAT and VAT by using the miRNeasy Mini Kit (Qiagen). Briefly, around 30 mg of liver or heart stabilized in RNAlater and 100 mg of AT in cryogenic tubes or in RNAlater were homogenized in M-tubes (Miltenyi Biotec) containing 1 ml QIAzol Lysis Reagent (Qiagen) and using a gentleMACS Dissociator (Miltenyi Biotec). Following this, 200 µl chloroform was added to the homogenate and subsequently centrifuged (15 min, 14000 rpm) whereafter 450 µl of 100% ethanol was added to the upper, aqueous phase. For the AT, before adding chloroform, an extra step was performed: centrifugation for 10 min at max speed at 4°C to remove the fat residues[26]. The RNA was then purified through a column-based process, including a DNase treatment on-column, to eliminate gDNA, using RNase-free DNase Kit (Qiagen), according to the manufacturer's protocol. Purity and RNA yield were measured on a NanoDrop (Spectrophotometer ND-1000, Thermo Scientific) and RNA integrity (RIN) was evaluated on an Agilent 2100 Bioanalyzer (Agilent Technologies) using the Agilent RNA 6000 Nano Kit (Agilent Technologies), according to the manufacturer's instructions. All samples showed an $A_{260/280}$, ratio between 1.9 and 2.2, but only samples with a RIN above 6.5 were selected for RNA-seq. Ribosomal RNA (rRNA) depletion stranded cDNA library construction and 100 bp paired-end sequencing were performed by an external provider using the DNBSEQ platform (BGI-Wuhan NGS Lab). Detailed information on RNA samples and sequencing quality control (QC) for each sample is provided in supplementary file 1. Several RNA samples were not submitted to BGI due to poor quality, primarily based on low RIN. Additionally, some samples submitted to BGI QC failed to meet RIN criteria and were not processed further. In total, 11 VAT, 11 SAT (Control = 4, MC-HFD = 7 for both depots), 10 liver (Control = 5, MC-HFD = 5) and 7 heart (Control = 4, MC-HFD = 3) samples went through library preparation.

RNA-seq analysis

Raw sequencing data was filtered by BGI using the SOAPnuke pipeline[27], with the following parameters enabled:"-n 0.001 -l 20 -q 0.4 --adaMR 0.25 --polyX 50 --minReadLen 100. Quality assessment of this data was subsequently performed using multiqc[28]. Except for two samples excluded due to excessive duplication levels, all 37 samples passed QC (see supplementary file 2). Reads were mapped to the *Sus scrofa* reference transcriptome (Ensembl release 110) using Salmon[29](v1.10.2). As Ensembl provides separate fast file for cDNA and ncRNA, these were concatenated to generate the full transcriptome. Prior to quantification with Salmon, an index was generated incorporating the genome to create decoy sequences, enabling more accurate handling of reads originating from unannotated regions. Libraries were then mapped to this index using Salmon quant, with the following parameters enabled: --gcBias, --seqBias, --validateMappings, --numGibbsSamples 100, --useEM and --rangeFactorizationBins 4.

Prior to analysis, transcripts annotated as rRNA were removed, resulting in libraries with a median read depth of 24 million reads (mean = 25 million, min = 12 million, max = 39 million). Detailed information regarding mapping and library size for each sample is available in supplementary file 3. Technical overdispersion arising from read-to-transcript ambiguity was estimated with edgeR[30]. Transcript counts were subsequently scaled by these estimates to produce counts suitable for input into established tools for gene-level analysis.

For exploratory analysis, lowly expressed transcripts were filtered out using filterByExpr in edgeR, with the default settings, and expression values were normalized and log2-transformed using cpm in edgeR. Principal component analysis (PCA) was then performed using prcomp in stats, with default parameters, and ellipses were computed with stat_ellipse assuming a multivariate normal distribution. Differential expression analysis was performed using linear models in limma, following variance stabilization with voom[31]. Sample quality weights were estimated and included in the modelling. PCA revealed that the overall expression patterns of VAT and SAT were roughly similar (Fig. 4A). Based on the PCA, we then first included an interaction between the MC-HFD diet and tissue type in our model, but failed to detect a significant interaction effect, indicating that both tissues responded similarly to the MC-HFD diet. Therefore, we proceeded to build separate models for each of the four tissue types using the diet group as the independent variable, which estimates the difference in expression between MC-HFD and control samples. For each design, an edgeR object was built using the raw counts. Lowly expressed transcripts were filtered using the filterByExpr, now accounting for the specific design matrix, and normalization was performed using the trimmed mean of M-values (TMM) method. Statistical testing was computed by eBayes in limma, and transcripts were considered differentially expressed (DE) when $|\log_2 FC| \geq 1$ and adjusted P-value < 0.05. Benjamini-Hochberg (BH) was used to correct for multiple testing. Volcano plots were visualized with ggplot2 and heatmap using ComplexHeatmap package[32]. For subsequent enrichment and network analysis, differentially expressed transcripts (DETs) were aggregated to gene-level, where a gene was classified as DE if at least one of its isoforms exhibited differential expression.

Overrepresentation analysis of DETs

We performed overrepresentation analysis (ORA) to identify enriched Gene Ontology (GO) terms and Kyoto Encyclopedia of Genes and Genomes (KEGG) pathways among the DE results using clusterProfiler (v4.13.4)[33]. GO annotations were categorized into biological processes (BP), molecular function (MF) and cellular component (CC). Ensembl gene identifiers were mapped to Entrez ID using biomaRt (v2.61.3)[34]. Genes that could not be mapped to an Entrez ID or lacked functional annotation were excluded from the analysis. For each tissue, separate analyses were conducted for significantly upregulated and downregulated genes. As the background set, we used the list of all expressed genes in each tissue with known annotation. Gene sets with a minimum of 10 and a maximum of 500 genes were considered in the analysis, and significance thresholds were set at adjusted P-value < 0.05, calculated via BH method. Visualizations were generated with genekitr (v1.2.8). In order to reduce redundancy and improve interpretability among the significantly enriched GO terms, quickGO[35] web tool was used to evaluate the hierarchical structure of GO annotations. In case of terms included in the same ancestor chart, the most specific term was selected for summarizing the results in the figure. For KEGG annotations, enriched terms were ranked by adjusted P-value, and the top five terms were selected for representation.

Protein-protein interaction network of DETs

A protein-protein interaction (PPI) network of DE results was generated using STRING database (https://string-db.org/) and visualized in Cytoscape software (v3.10.3). Only interactions with a confidence score above 0.4 (medium confidence) were retained. In the network nodes represent proteins and edges indicate functional or physical protein interactions. Clusters of interconnected nodes were identified using MCL plugin[36], with granularity parameter of 3, followed by group-wise functional enrichment using GO and KEGG annotations, using the initial network as the background set. A redundancy threshold of 0.7 was used to filter out similar terms. CytoHubba plugin was employed to rank nodes based on the maximal clique centrality (MCC) degree algorithm[37], and the top 30 nodes were selected. The STRING-disease feature was used to generate a network using the term obesity (DOID:9979), applying a confidence score threshold of 0.4 and limiting the network to 300 proteins. Overlap analysis between this and each tissue-derived network was performed, and a hypergeometric test from the stats package was used to determine whether these were overrepresented in our data. As the background set, we used the list of all genes expressed in each tissue with annotation in STRING database. A similar approach was taken to assess the overrepresentation of obesity-related genes identified through text mining of pig-related obesity studies. Here, for the background set we used the list of all protein-coding genes expressed in each tissue.

Correlation analysis

Correlations between transcript expression levels and phenotypic parameters were explored using spearman's method from the stats package (v4.4.1), with missing values excluded on a pairwise basis. Expression values were normalized and log2-transformed prior to analysis. For genes with multiple isoforms, the one exhibiting the lowest adjusted P-value was selected for analysis. Statistical significance of the correlations was evaluated using rstatix package, and P-values were adjusted for multiple testing using BH method. The results were visualized using ggcorrplot.

Data analysis and statistical tests

Statistical analysis and data visualization of morphometric parameters, adipocyte area and biochemical measurements were performed using the software GraphPad Prism v10. Repeated measures two-way ANOVA was used to test the interaction effect of week and diet. Statistical significance between control and MC-HFD group at individual time points was evaluated with Welch´s unpaired t-test for normally distributed data. P-values were adjusted for multiple comparisons using the Holm-Šídák correction. For data not normally distributed Mann-Whitney U test was used. Data normality was evaluated using Shapiro-Wilk test. The same approach was used for testing differences between diet groups in adipocyte area for each depot.

Upstream processing of RNA sequencing data was performed using Unix terminal and downstream analysis was performed using R v4.4.1 and RStudio 2024.09.0 + 375.

Results

Phenotypic characteristics of MC-HFD Ossabaw pigs

Weight curves for both groups are shown in supplementary Fig. 1S. As mentioned, two pigs, pig no. 1 from control and pig no. 30 from MC-HFD group, exhibited unusual weight curves and were therefore excluded from the sequencing sample set and are excluded from the data sets in Fig. 2 and Fig. 3. After 11 weeks of obesogenic feeding, the MC-HFD group demonstrated a significant increase in BW, ABC, BMI and BSA compared to the control group (Fig. 2A, $P < 0.001$; 2B, $P = 0.047$; 2C, $P < 0.001$; 2D, $P = 0.001$). Concerning dyslipidemia-related parameters, circulating triglyceride remained unchanged between the groups, while concentrations of total cholesterol were significantly higher in MC-HFD pigs than in control pigs at week 11 (Fig. 3B, $P = 0.03$). Cholesterol transporting lipoproteins exhibited a significant interaction effect (supplementary Table 1S), with HDL concentrations significantly higher in the MC-HFD group compared to the control group (Fig. 3D, week 11, $P = 0.008$), while circulating LDL revealed only a tendency to higher concentrations in week 11 (Fig. 3C, $P = 0.16$). No evidence of insulin resistance was observed, as determined by HOMA-IR (data not shown), based on unaffected fasting glucose and insulin concentrations (Fig. 3F and Fig. 3G). Additionally, long-term glucose homeostasis appeared preserved in the MC-HFD group, as indicated by no change in fructosamine levels (Fig. 3E). Likewise, the serum concentrations of CRP, an established inflammation biomarker, displayed no reaction to the diet over time (Fig. 3H). The reason for the elevated levels of this protein at week − 4 in both groups, particularly in the MC-HFD group, remains unclear. Histological analysis revealed a significant increase in average adipocyte area in both AT depots in the MC-HFD group compared to the control group (Fig. 3I, SAT, $P = 0.026$; VAT, $P = 0.004$), consistent with adipocyte hypertrophy. A representative example of this difference is shown in supplementary Fig. 3S.

Tissue-specific transcriptomic profiles evaluated by PCA

PCA was used to visualize transcriptomic profiles from the four different tissues collected from control and MC-HFD pigs at the end of the study. Primary clustering was driven by tissue type rather than dietary group (Fig. 4A), highlighting strong tissue-specific transcriptional signatures. The two AT depots showed similar overall expression profiles, as confirmed by the ellipses (Fig. 4A), and no interaction of tissue type with diet was demonstrated for these tissues (results not shown). Individual PCA plots are shown only for tissues which showed significant differential expression (see supplementary Fig. 4S for heart and SAT PCA plots). PCA analysis for liver samples showed partial separation between diet groups, mainly along PC2. However, considerable within-group variation was present, particularly among control samples, as indicated by the large blue ellipse in Fig. 4B. For VAT samples, a clear separation according to the diet group was observed along PC2, however, the ellipses for control and MC-HFD still overlapped, indicating some spread within each group.

Differential expression analysis between control and MC-HFD pigs

Differential expression analysis comparing MC-HFD vs. control was performed for each tissue type separately, and results were visualized using volcano plots and hierarchical heatmaps. The extensive results are available in supplementary file 4. While heart and SAT exhibited no significant transcriptional changes in response to the diet, the liver showed a modest response, with only 40 transcripts significantly regulated in MC-HFD compared to control group (Fig. 5B). Approximately three times more DETs were upregulated than downregulated (up = 31, down = 9). Hierarchical clustering revealed a distinct diet group-driven differentiation, demonstrating high consistency within each diet group (Fig. 5D). VAT displayed robust transcriptional alterations in response to the obesogenic diet, with a total of 666 DETs in the MC-HFD group compared to the control group (Fig. 5A). Unlike the results for liver, downregulated transcripts dominated with the number of upregulated DETs being roughly half that of downregulated DETs. A clear separation between groups was also visible in the heatmap, however the MC-HFD group showed more heterogeneous expression patterns, particularly evident in pigs number 25 and 29 (Fig. 5C). Only one transcript, fatty acid synthase (FASN) was differentially regulated in both VAT and liver (downregulated in both tissues), underscoring the highly tissue-specific transcriptional responses of VAT vs. liver in response to 11 weeks of MC-HFD feeding. A possible reason for the lack of differential regulation in the heart could be a combination of high within-sample variability, as observed in the PCA (supplementary Fig. 4S B), and the low number of biological replicates (control = 4, MC-HFD = 3), making it more challenging for the model to distinguish within-group from between-group variability. Whereas the results showed a large number of DETs in VAT, none were found in SAT. This suggests that the dietary intervention induced transcriptomic-level changes in VAT that were strong enough to be detected as statistically significant. In contrast, while the diet may have also caused some changes in SAT, the effect was likely weaker, as indicated by the absence of clear separation between the diet groups in the PCA (supplementary Fig. 4S A), and did not reach statistical significance.

While the RNA-seq data are resolved and statistically tested at the transcript level (forming the basis of the PCA plots, volcano plots and heatmaps (Figs. 4 and 5)), we aggregated the data to the gene-level for subsequent enrichment and network analysis to obtain a gene level overview of the impact of obesity on gene expression (Figs. 6–10).

GO and KEGG enrichment analysis

For each tissue dataset, DETs aggregated at the gene level were further explored through functional and pathway enrichment analysis using GO and KEGG annotations. GO analysis for VAT showed that upregulated genes were dominated by terms associated with protein synthesis, such as cytosolic large/small ribosomal subunit, cytoplasmic side of rough endoplasmic reticulum membrane and structural constituent of ribosome, and terms related to mitochondrial electron transport chain, spliceosome and extracellular matrix. In contrast, the downregulated genes in VAT, although twice as many as the upregulated genes, yielded limited enrichment results, with only two significant terms identified within the CC (cellular component) category associated with G-protein complex and neuro compartments (Fig. 6A). In the liver, negative regulation of cell growth, plasma lipoprotein associated processes and glycosaminoglycan binding were overrepresented among upregulated genes, while downregulated genes were significantly involved in metabolic processes including fatty acid biosynthesis and amino acid catabolic processes (Fig. 6B). KEGG analysis revealed that in VAT, pathways including oxidative phosphorylation, ribosome, thermogenesis, and diabetic cardiomyopathy were significantly overrepresented among upregulated genes, whereas downregulated genes were enriched only in glutamatergic synapses pathway (Fig. 6A). In the liver, upregulated genes were involved in hormone signaling and cholesterol metabolism, while pathways such as arginine biosynthesis, fatty acid metabolism, alcoholic liver disease and AMPK signaling pathway were overrepresented within the downregulated genes (Fig. 6B). For both tissue datasets, KEGG pathway analysis showed concordance with GO enrichment results. The complete results are available in supplementary file 5.

PPI network analysis

VAT

The interactions between VAT DETs aggregated at the gene level were explored with a PPI network constructed using STRING database and visualized in Cytoscape (see supplementary Fig. 5S). A total of 472 nodes and 815 edges were identified, with the interactions showing a significant enrichment ($P = 1.15\times10^{-8}$), likely reflecting biologically meaningful and coordinated transcriptional responses in our study. The MCL algorithm identified 28 clusters (minimum group size = 4) within the network, of which seven were selected for further analysis (Fig. 7). The selection was based on clusters that were involved in processes or pathways also identified in the overrepresentation analysis. Functional associations for each cluster were obtained using KEGG and GO annotations. The list of terms identified for each cluster is provided in supplementary file 6. As multiple terms were identified for each cluster, the term used to annotate each cluster was chosen according to statistical significance, specificity and the extent of node coverage. In Fig. 7, the nodes belonging to the term used to annotate the cluster are highlighted with a blue border. **Cluster 1** was primarily linked to translation (RPL = 8, RPS = 6, EEFSEC and EIF = 3), while **cluster 2** was strongly associated with oxidative phosphorylation (NDUF = 8, COX = 2 and ATP5 = 3). **Cluster 3** showed an enrichment in G protein-coupled receptor (GPCR) signaling pathway (GN = 6, GRK2, GABBR1, ADRA2A, HCAR2 and PTAFR), whereas **cluster 4** was significantly associated with extracellular matrix (ECM) structural constituent (COL1A1, COL6A5, COL6A1, COL22A1 and COL27A1). **Cluster 5** was significantly associated with spliceosomal complex (LSM8, SNRP = 4, RNF113A and PPIL2), and **cluster 6** was enriched in ECM (LOX, MFAPs = 2 and FBLN5). **Cluster 7**, despite no significant GO or KEGG enrichment, was selected due to the presence of FASN, the only gene regulated in both tissues. Notably, three of the nodes (FASN, FABP4 and SLC27A1) are known to be involved in fatty acid metabolism. Furthermore, nodes in the network were ranked using the MCC algorithm in cytoHubba plugin to screen the top 30 hub genes. These mainly included nodes belonging to cluster 1 and 2 (Fig. 8), highlighting the centrality of these processes in VAT regulation following 11 weeks of MC-HFD feeding.

LIVER

Similarly, a PPI network was constructed again to investigate the interactions between DE results detected within liver samples (Fig. 9). A total of 28 nodes and 5 edges were identified, with the interactions demonstrating a significant enrichment (P = 0.0131), suggesting biologically meaningful responses in our study, although with a low level of connectivity. Enrichment analysis to annotate the subnetworks was performed as previously mentioned. The list of terms identified for each cluster is provided in supplementary file 6. **Subnetwork 1** was enriched in fatty acid biosynthetic process, **subnetwork 3** was linked to arginine biosynthesis and **subnetwork 4** was associated with thyroxine 5-deiodinase. **Subnetwork 2**, consisting of two lipases, showed no significant results. Interestingly, the expression of FASN, an enzyme that catalyses the biosynthesis of saturated fatty acids[38], and SCD, involved in the synthesis of monounsaturated fatty acids (MUFAs)[39], was downregulated in MC-HFD vs. control, while expression of ELOVL2, an essential enzyme for elongation of long-chain polyunsaturated fatty acids (PUFAs)[40], was increased. In addition, DIO1, ARG1, LIPG and ELOVL2 were included in the top 10 DETs ranked by adjusted P-value.

Associations with obesity-related genes

We assessed the association between DE results identified in this study and obesity-related genes, using both the top 300 genes from STRING human disease database, and genes identified through text mining of pig-related obesity studies (see supplementary file 7). In the case of VAT, this revealed a total of 7 genes overlapping with the STRING list (fold enrichment = 0.9, P = 0.63) and 11 genes overlapping with the pig-related list (fold enrichment = 1.3, P = 0.27), amounting to 15 unique genes (see full list of genes in supplementary file 7). Overall, this suggests limited changes in obesity-related genes for VAT. In the liver, the analysis revealed a total of 3 genes overlapping with the STRING list (fold enrichment = 6.3, P = 0.01) and 5 genes overlapping with the pig-related list (fold enrichment = 8.6, P = 0.0003), yielding a total of 6 unique genes (FASN, SCD, DIO2, DIO1, PCSK9 and GHR). Unlike the findings in VAT, these results indicate that a higher degree of genes commonly associated with obesity are dysregulated in the liver. In Fig. 7 and Fig. 9, obesity-related genes found at the intersection are highlighted in pink.

Associations between phenotype and genes representing core findings

For VAT, representative genes were selected on a cluster basis, considering known associations with obesity, inclusion among the top 30 hub, or presence in the term used to annotate the cluster prioritized by adjusted P-value, resulting in the following VAT genes: RPS29, RPL34, EEFSEC, COX7C, NDUFV2, ATP5MF, CPE, COL1A1, COL6A1, MGP, GNAI2, GRK2, GABBR1, SNRPD2, RNF113A, LSM8, LOX, FBLN5, MFAP4, FABP4, FASN and SLC27A1. For liver, a focus was given to the genes showing at least one interaction in the network: SCD, FASN, ELOVL2, LIPN, LIPG, ARG1, GLUD1, DIO2 and DIO1.

To investigate potential associations between selected genes for each tissue and phenotypic parameters, correlation analyses were conducted (Fig. 10). This analysis considered the phenotypic parameters that exhibited statistically significant differences between dietary groups, i.e. BW, ABC, BMI and BSA (see Fig. 2) and HDL, Cholesterol, SAT and VAT adipocyte area (see Fig. 3). Starting with VAT (Fig. 10A), genes encoding for ribosomal proteins (RPs) and the translation elongation factor (EEFSEC) showed significant correlations with all four morphometric parameters, emphasizing a strong relationship between their expression and the phenotype of the MC-HFD pigs. Although significance was less consistent, genes involved in oxidative phosphorylation demonstrated positive associations with the MC-HFD pig phenotype. Moreover, the gene encoding for carboxypeptidase E (CPE) was found to be significantly associated with BW, BMI, BSA and visceral adipocyte area. GPCR signalling-related genes showed significant negative correlations with all four morphometric parameters. With regards to collagen-encoding genes, decreased expression was significantly and negatively correlated with most morphometric traits of the MC-HFD pigs. Of the other ECM-related genes, MGP and LOX showed strong and positive associations with morphometric parameters and visceral adipocyte area. MFAP4 and FBLN5 also showed some significant associations, further suggesting an involvement of ECM components in the phenotype of MC-HFD pigs. Overall, genes associated with the spliceosome demonstrated a strong positive association with the traits of MC-HFD pigs. Lastly, among the genes involved in fatty acid metabolism, FASN and SLC27A1 demonstrated inverse associations with the phenotype, although not significant for all phenotypic traits. In the liver (Fig. 10B), genes related to fatty acid biosynthesis exhibited a general trend of inverse association with the phenotype, while not consistently reaching significance across all morphometric traits. Similarly, expression of LIPG and LIPN, genes encoding for lipid-hydrolysing enzymes, demonstrated mostly strong and positive correlations with morphometric parameters. Notably, increased expression of ELOVL2 and LIPN was strongly and positively associated with greater subcutaneous adipocyte area in MC-HFD pigs. Finally, ARG1 and DIO1 expression was strongly correlated with BW, BMI and BSA, with ARG1 showing also a significant and inverse association with visceral adipocyte area. For details on correlation coefficient and statistical significance see supplementary file 8.

Discussion

The current study aimed at investigating tissue-specific signatures at the transcriptomic level, following a 11-week diet intervention with increased calories, fat, fructose and cholesterol, using the Ossabaw pig as a model for human obesity. Four metabolism-relevant tissues, liver, heart, visceral and subcutaneous white adipose tissue, were chosen for deep RNA sequencing analysis. We established that Ossabaw pigs subjected to a relatively short duration obesogenic diet with medium cholesterol content (MC-HFD) exhibited a 42% increase in BW relative to the control animals. While body composition was not assessed, the MC-HFD pigs also exhibited a significant increase in ABC. This morphometric parameter has been suggested to correlate significantly with visceral fat in this pig breed[(6)], providing evidence of central obesity in this experiment. Currently, there is no accepted index to quantify truncal adiposity in pigs, although BSA has been used by Curtasu[(41)] and BMI by Neeb[(21)] as an additional measure. In this study, both parameters were increased in MC-HFD pigs, when compared to the controls. Consistent with increased adiposity, adipocyte expansion by hypertrophy was observed both in SAT and VAT, a change associated with adipocyte dysfunction and consequently adverse metabolic outcomes[(42)]. Concerning lipid levels in circulation, overt dyslipidemia was not observed, although cholesterol increased, LDL only tended to increase and HDL also increased in the MC-HFD group, and TG levels were unchanged. Even though dyslipidemia in pigs can involve increases in HDL, the rise in LDL is typically more pronounced[(6, 43)]. This was not the case in our MC-HFD pigs, as LDL/HDL was significantly decreased compared to the controls (results not shown). The 0.5% cholesterol content used in the present study is lower than recommended to induce significant changes in the lipid profile in pigs[(43)]. In fact, Ossabaw pigs fed a short-term (9–10 weeks) high fat diet with 2% cholesterol achieved increased LDL/HDL ratio[(6, 44)]. In addition, the MC-HFD diet did not result in insulin resistance, as assessed by HOMA-IR (results not shown), nor did it impair long-term glucose control, as confirmed by unaffected fructosamine levels. Dysregulation of insulin and glucose metabolism is usually demonstrated in the Ossabaw breed after 5–6 months of obesogenic diet, and typically a weight gain of 60% compared to matched controls is necessary[(43)]. The MC-HFD diet used here was also used to induce obesity in adolescent Gottingen minipigs[(18)]. In that study and in contrast to the present study, the feeding was performed *ad libitum* for the MC-HFD group and restricted for the control pigs (250g/day), for a period of 12 weeks and MC-HFD fed animals were found to be 2.4 times heavier than the control and showed increased LDL/HDL ratio, however, only a tendency to decreased insulin sensitivity (assessed by HOMA-IR) in MC-HFD males. The obtained dyslipidemia in this study[(18)] is most likely attributable to the ad *libitum* feeding in the MC-HFD group, which also resulted in a substantial weight and body fat (~ 40% attained in MC-HFD) difference between the groups, likely accelerating the metabolic disturbances.

The absence of dyslipidemia, insulin resistance and glucose intolerance, despite evidence of increased body fat accumulation, is characteristic of a human obesity sub phenotype referred to as metabolically healthy obesity (MHO)[(42)] which has been demonstrated previously in Ossabaw pigs[(44, 45)]. The presence of hypertrophic adipocytes without evidence of metabolic disturbances, including no clear signs of dysregulated lipolysis at the expression level, may support the notion that adipocytes are expandable at least until a certain point. Furthermore, the serum concentration of CRP, a marker of inflammation and obesity[46], was not increased. Adipokine data showed a non-significant trend toward increased serum leptin in MC-HFD pigs at week 11 (supplementary Fig. 7S). Leptin is known to increase with adiposity in pigs, similar to humans[47, 48]. In contrast, adiponectin, also reported to be regulated with obesity in pigs[47, 48], was unaffected by MC-HFD feeding (supplementary Fig. 7S). Therefore, based on the phenotypic data we suggest that the MC-HFD pig model represents an obese, pre-MetS state.

Transcriptomic signatures analysed in diet-induced obesity studies in pigs have been widely conducted, however, in most cases, achieving a MetS state[12–16]. Although a couple of studies have described partial MetS states in obese Ossabaw pigs[44, 45], this, to our knowledge, is the first study to characterize global transcriptomic changes in liver and VAT in a model believed to represent an obese, pre-MetS state.

Despite hypertrophic adipocytes being present in SAT, no DETs were found in this tissue. Previous studies have also reported fewer transcriptional changes in SAT than in VAT when comparing obese with non-obese individuals[49]. The smaller number of DETs observed in the liver compared to VAT confirms the primary role of adipose tissue in responding to lipid and energy surplus, making it more transcriptionally dynamic, whereas the liver, as being central to metabolic regulation, can be expected to show a more modest transcriptional response in the early state of obesity. Supporting this, we found only a single shared DET (FASN) between the two tissues, which emphasizes the highly tissue-specific nature of the early response to obesity. On the other hand, DE results in liver were strongly enriched in obesity-related genes, while this was not the case in VAT. This suggests that, although the liver may exhibit a more limited response, the changes it undergoes are more strongly aligned with alterations typically associated with obesity. Thus, overall, the significantly enriched and densely connected network for VAT points to a robust and highly coordinated response to the MC-HFD diet, involving processes not captured by the obesity gene sets used. These observations align with results in mice, where metabolic complications resulting from obesity first showed up in the liver and then in the AT[17].

We found FASN expression was 3-fold (VAT) and 2.4-fold (liver) lower in MC-HFD than in control pigs. Decreased expression of this lipogenic enzyme was also reported for human overweight and obese subjects[50]. In line with this, dietary fats have been reported to inhibit *de novo* lipogenesis (DNL) in AT in pigs[51], however another study found that pigs fed *ad libitum* with the MC-HFD diet showed increased expression of lipogenic genes[18]. Growing evidence links DNL products to maintenance of insulin sensitivity[52], and we also identified the downregulation of a cluster highly associated with insulin signalling pathway in the VAT network. Thus, our findings suggest that obesity is associated with both downregulation of DNL and impairment of insulin signalling in VAT. Curtasu[41] and Polakof[53] did not report an increase in hepatic FASN expression after a high fat and high fructose diet in minipigs. Increased intake of dietary fat inhibits liver FASN expression[38], and we also find negative correlations between obesity (morphometric parameters) and the expression of FASN as well as with SCD, an enzyme suggested to promote DNL[54]. On the other hand, increased expression of liver FASN has been linked to insulin resistance and liver steatosis in obese subjects[55]. We hypothesize that in the MC-HFD pigs, the hepatic downregulation of enzymes essential for DNL is a mechanism to maintain hepatic lipid homeostasis.

VAT DET enrichment and network analysis

As noted above adipocytes of the VAT were significantly enlarged in the MC-HFD pigs. Enrichment and network analysis of DE results in VAT revealed an upregulation of the oxidative phosphorylation pathway, with several genes encoding mitochondrial respiratory chain enzymes identified among the top 30 hub genes, indicative of mitochondrial activation. Whole blood transcriptomics of healthy obese (no MetS) showed that oxidative phosphorylation pathways were upregulated in comparison with healthy lean individuals[56]. Also, non-diabetic obese individuals were found to maintain or elevate mitochondrial function, while individuals with T2D and NAFLD exhibit reduced hepatic ATP production and mitochondrial dysfunction[57], consistent with downregulation of electron transport chain genes in VAT of obese women with T2D but not if T2D was not present[49]. This suggests that mitochondrial dysfunction is associated with advanced MetS. Thus, the increase in mitochondrial oxidative capacity observed in our data suggests a metabolically healthy reaction to excess lipid influx. Preliminary data (see supplementary Fig. 6S A) pointed to an increase in beige adipocytes in VAT of MC-HFD pigs, indicative of energy uncoupling. Pigs have a non-functional UCP1 gene, which in most mammals is responsible for energy uncoupling, however, the existence of beige adipocytes has been reported in pigs[58]. Notably, KLF11, a gene responsible for inducing the differentiation of beige adipocytes has been found significantly upregulated in the MC-HFD pigs. Beige adipocytes are associated with improved metabolic health[59], further supporting the notion that MC-HFD pigs undergo a healthy remodelling of AT in response to high lipid intake. In contrast with our findings, studies by Chattopadhyay[60] and Yin[61] reported reduced mitochondrial oxidative capacity in SAT from obese human individuals, compared with control subjects. In addition to putative species-specific differences, this discrepancy could be attributed to differences in adipose tissue depots, in metabolic health and/or in the methods employed (transcription vs. activity).

The analysis of DE results in VAT also revealed a significant enrichment of processes associated with protein synthesis, with 13 upregulated ribosomal protein (RPs) genes, key components of ribosome biogenesis, identified among the top 30 hub genes, some of which also significantly correlating with the morphometric parameters and supported by human evidence[56, 62]. We observed both upregulation (EIF3H) and downregulation (EIF3L, EIF4H, EEFSEC) of translation initiation and elongation factors, with EEFSEC expression showing a strong association with the MC-HFD phenotype. Taken together we hypothesize that the regulation of ribosomal proteins in VAT reflects an adjustment in the translational machinery necessary to support protein synthesis demands during adipocyte expansion[52], however no clear evidence for regulation of protein synthesis *per se.*

Our analysis also identified a cluster in VAT associated with GPCR signalling (cluster 3), in which most genes were downregulated and showed significant correlations with all morphometric traits. GRK2 encodes a kinase that phosphorylates the beta-adrenergic receptor, reducing its activity, and GNAI2 encodes a G-protein subunit that inhibits adenylate cyclase thereby decreasing cAMP levels. Beta-adrenergic receptor and cAMP signalling play a key role in stimulating lipolysis and regulating thermogenesis, and alterations in these pathways have been associated with obesity[63]. Thus, while our findings do not establish how GPCR signaling pathways are altered, they highlight the importance of processes modulating energy balance and fatty acid metabolism in the phenotype of MC-HFD pigs. This is supported by data from humans where GNAI2 and GRK2 were upregulated in obese adipose tissue, whereas expression of GABBR1 was unaffected[64, 65]. Notably, GNAI3, another adenylate cyclase inhibitor, was upregulated in MC-HFD pigs.

ECM remodelling is suggested to be associated with early phases of adipose tissue expansion[66]. In our data, VAT cluster 4 displayed significant downregulation of genes encoding collagens, the most abundant ECM protein class. Excessive and sustained deposition of collagen increases ECM rigidity, leading to ineffective storage of lipids and eventually promoting insulin resistance[59]. This is not seen in the MC-HFD pigs in our study, which is in partial contrast to human obesity where adipose expression of COL6A1 was found to be increased[64, 65]. Contrary to the collagen genes, LOX showed an increased expression and was significantly associated with a greater visceral adipocyte area in MC-HFD pigs. LOX is an enzyme crucial in fibrosis development, cross-linking collagen and elastin[67], and has been found increased in adipose tissue of obese individuals[64, 65]. This might suggest that in our pig model VAT is in a transitional state preceding persistent ECM expansion, which could explain why the matrix remodelling signature did not distinguish between the diet groups (see supplementary Fig. 6S B). Lastly, MGP, ranked as the top1 DET based on adjusted P-value, a matrix-associated protein calcification inhibitor, was significantly upregulated and showed strong correlations with all morphometric traits and visceral adipocyte area. This gene has been shown to be upregulated in human obesity[64, 65], and knockout studies in mice have demonstrated its important role in lipid turnover in adipocytes[68].

Both enrichment and clustering analysis revealed an overall upregulation of splicing machinery-associated genes, with some major spliceosome components (LSM8 and SNRDP2), and a minor spliceosome component (RNF113A) showing significant correlations with the morphometric parameters of the MC-HFD pigs. Downregulation of pre-adipocyte spliceosome genes has been demonstrated in obese individuals with insulin resistance, when compared with obese individuals[69]. Therefore, our findings seem to be consistent with the interpretation that the MC-HFD pigs represent a pre-MetS model.

Lastly, the cluster linked to fatty acid metabolism (cluster 7) in VAT showed an overall downregulation, except for FABP4, an intracellular chaperone for fatty acids and capable of activating lipase, increased levels of which have been strongly associated with obesity and insulin resistance[70]. Consequently, inhibition of FABP4 has been shown to increase insulin sensitivity[70]. However, no correlation between FABP4 upregulation and the phenotypic traits of the MC-HFD pigs was observed in our study. On the other hand, SLC27A1, also known as FATP1 (long-chain fatty acid transport protein) expression was significantly and inversely associated with some phenotypic parameters of the MC-HFD pigs, and it is shown to be downregulated in human obesity and associated with insulin resistance[64, 65]. In adipocytes, this protein translocates to the plasma membrane in response to insulin, facilitating cellular fatty acid uptake[71] and maybe promoting lipid accumulation in adipocytes[72]. Reduced expression of SLC27A1 in MC-HFD pigs could represent an early adaptive response aimed at limiting lipid storage in VAT. In mice, SLC27A1 knockout protected against diet-induced obesity and insulin resistance[73].

Notably, and in sharp contrast to what has been demonstrated in hypertrophic adipocytes[74], our results show no evidence of a distinct inflammatory environment in VAT from MC-HFD pigs (see supplementary Fig. 6S B), consistent with the phenotypic data showing no elevation in the levels of CRP in the MC-HFD group compared to the control. These findings further support the assumption that the MC-HFD pigs represent a pre-MetS model.

Liver DET enrichment and network analysis

No hepatic pathology (histology (data not shown)) was observed after 11 weeks of MC-HFD feeding. However, analysis of liver DE results revealed a significant enrichment of fatty acid biosynthetic process genes (subnetwork 1) among the downregulated genes in the MC-HFD group. While DNL related genes such as SCD and FASN were downregulated, ELOVL2, however, was upregulated and significantly correlated with BMI and subcutaneous adipocyte area. Studies in mice[75] and zebrafish[76] have shown that ablation of ELOVL2 indirectly led to transcriptional activation of DNL resulting in marked hepatic lipid accumulation and development of fatty liver disease[76]. Thus, the observed upregulation in the liver of MC-HFD pigs might downregulate lipogenesis. Although our data do not unveil the balance between lipid/fatty acid uptake, biosynthesis, oxidation, and secretion, we speculate that the observed regulation of SCD, FASN and ELOVL2 may reflect a protective mechanism aimed at maintaining hepatic lipid homeostasis. Liver´s subnetwork 2 was not functionally enriched in any GO or KEGG terms, however, the genes, particularly encoding for endothelial lipase (LIPG), were strongly associated with the phenotype of the pigs. In the liver, LIPG plays a central role in hydrolysing HDL-associated phospholipids for cholesterol clearance[77]. In contrast to findings in humans and mice, where LIPG expression typically shows an inverse correlation with HDL levels[77], we observed increased hepatic expression of LIPG alongside elevated HDL concentrations, although no direct correlation was detected. This might suggest species-specific differences in HDL metabolism, as also indicated by the generally observed tendency for increased HDL levels in dyslipidemic pigs[6, 21, 43]. However, LIPG expression was significantly correlated with all morphometric traits of the MC-HFD pigs, suggesting it reflects a broader response to lipid imbalance. Another process found dysregulated in the liver of our MC-HFD-fed pigs was amino acid metabolism (subnetwork 3), with a coordinated downregulation of ARG1 and GLUD1, key enzymes in the urea and the TCA cycle, respectively[78], hence maybe reflecting a shift away from amino acid catabolism. Inhibition of ARG1 has been shown to reduce hepatic lipid accumulation[79] and the observed downregulation of ARG1 might function to secure availability of hepatic L-arginine, possibly to maintain NO production. In addition, amino acids play a central role in supplying carbon for hepatic TCA cycle and fatty acid synthesis at least in mice, and thus reduced amino acid catabolism could limit lipogenesis[80]. Notably, ARG1 expression was significantly and negatively correlated with several phenotypic traits of the MC-HFD pigs, also suggesting this gene to be associated with hepatic responses to increased lipid burden. Lastly, deiodinase activity represented by both DIO1 and DIO2 (subnetwork 4) was significantly upregulated in MC-HFD pigs. Here, only DIO1 expression was positively correlated with phenotypic traits, specifically BW, BSA and BMI, suggesting an increased association with body size rather than with more direct measures of adiposity, such as ABC or adipocyte area. In obese mice, hepatic DIO1 expression and activity were increased, coinciding with lipid accumulation in the liver, and liver-specific knockdown of DIO1 combined with an obesogenic diet resulted in increased hepatic triglycerides and cholesterol when compared to wild-type, obesogenic-fed mice[81]. Thus, the observed increase in hepatic DIO1 may reflect an early mechanism in response to the lipid influx aimed at preserving liver homeostasis in the MC-HFD pigs.

However, several limitations should be considered when interpreting the findings. The relatively small number of animals included in the experimental groups limits the generalization of our findings. Furthermore, key metabolic organs such as skeletal muscle and brain were not included in this study, limiting our ability to assess whole-body metabolic adaptations in response to the diet intervention. The inclusion of male castrated pigs may not capture the full spectrum of metabolic responses, as sex differences in metabolic responses are well documented, thus, limiting the generalization of our results.

Overall, we propose that metabolic flexibility is still preserved at this stage in MC-HFD pigs. However, additional functional studies are required to determine whether the observed molecular changes represent compensatory adaptations or early indications of metabolic dysfunction.

Conclusions

This study provides a detailed characterization of early transcriptomic adaptations associated with increased adiposity preceding the onset of systemic metabolic dysfunction. The MC-HFD pigs developed truncal obesity, as indicated by a modest but statistically significant increase in ABC and marked adipocyte hypertrophy in SAT and VAT, while maintaining a metabolically healthy status. The limited changes observed in obesity-related transcripts in VAT, particularly the absence of inflammation, support the classification of MC-HFD pigs as being in a pre-MetS state. In VAT, we propose that transcriptional alterations related to energy metabolism reflect adaptive responses to increased lipid intake, while modifications in ECM components suggest a transitional state preceding sustained matrix expansion. At the same time, changes in lipid metabolism may represent compensatory mechanisms aimed at preventing adipocyte overfilling, accompanied by early signs of altered insulin signalling. In contrast, the liver exhibited a transcriptional profile more closely linked to obesity, showing strong evidence of suppressed DNL-associated transcripts, potentially reflecting an adaptive mechanism to preserve hepatic lipid homeostasis, which is consistent with the absence of histopathological abnormalities.

Declarations

Acknowledgments

We thank the DTU European Ossabaw Facility animal caretakers for all animal work, Berit Ø. Christoffersen, Novo Nordisk for having performed measurements on blood chemistry parameters, Henriette Vorsholt for the support in the laboratory, Nisanicca Jeevendra for performing glucose and insulin measurements, Susanne Primdahl for preparing the slides for histology analysis, Louise Ramhøj for facilitating the Pannoramic Midi II digital slide scanner and Grigorii Nos for computing the gene signature scores. The study was supported by the DTU European Ossabaw Facility. Histology images were generated though accessing research infrastructure at DTU National Food Institute, including FOODHAY (Food and Health Open Innovation Laboratory, Danish Roadmap for Research Infrastructure).

Author contributions

P.H. designed the animal experiments and coordinated the study. C.V. performed the literature review, RNA extractions, analysed and interpreted the results. K.K and T.J.G. analysed histology images. B.L revised the differential expression analysis under supervision by J.G. C.V. and P.H. prepared the manuscript. All authors reviewed the written manuscript.

Funding

The study was funded by the DTU Health Technology department and DTU European Ossabaw facility. RNA sequencing associated costs were funded by Brødrene Hartmanns Fond and Kong Christian den Tiendes Fond. BL and JG were supported by the Novo Nordisk Foundation (NNFSA210073688). KBK was funded in part by the Austrian Science Fund (FWF) 10.55776/J4822 and TJG was supported by Novo Nordisk Foundation (NNF21OC0067271) and the Independent Research Fund Denmark (2100-00047B). The funders did not have any influence on the design of the study, the analyses and interpretation of the study results and in writing the manuscript.

Competing interest

All authors declare no conflicts of interests.

Ethics declarations

The study was approved by the Danish Animal Experiments Inspectorate (permit 2016-15-0201-01022) and complies with the ARRIVE guidelines. The experimental procedures were performed in accordance with Danish laws and regulations regarding the use of animals in research (The Danish Ministry of Justice, Act on Animal Experiments no. 474 of 15 May 2014, as stipulated in the executive order no. 12 on 7 January 2016), and all animal handling complied with DTU's Animal Welfare Policy. All animals were obtained from the Ossabaw facility at the Technical University of Denmark (https://ossabaw.dtu.dk) and housed at the University of Copenhagen animal facility. The experiments were specifically approved by the institutional animal ethics committee at University of Copenhagen as project number P 19-409.

Consent to participate: Not applicable.

Consent for publication: Not applicable.

References

1. Obesity. and overweight [Internet]. [cited 2025 June 18]. Available from: https://www.who.int/news-room/fact-sheets/detail/obesity-and-overweight
2. World_Obesity_Atlas_2025_Press_Release.pdf [Internet]. [cited 2025 June 18]. Available from: https://s3-eu-west-1.amazonaws.com/wof-files/World_Obesity_Atlas_2025_Press_Release.pdf
3. Rubino F, Cummings DE, Eckel RH, Cohen RV, Wilding JPH, Brown WA, et al. Definition and diagnostic criteria of clinical obesity. Lancet Diabetes Endocrinol. 2025;13(3):221–62.
4. Kleinert M, Clemmensen C, Hofmann SM, Moore MC, Renner S, Woods SC, et al. Animal models of obesity and diabetes mellitus. Nat Reviews Endocrinol. 2018;14(3):140–62.
5. Cluzel GL, Ryan PM, Herisson FM, Caplice NM. High-fidelity porcine models of metabolic syndrome: a contemporary synthesis. Am J Physiology-Endocrinology Metabolism. 2022;322(4):E366–81.
6. Dyson MC, Alloosh M, Vuchetich JP, Mokelke EA, Sturek M. Components of Metabolic Syndrome and Coronary Artery Disease in Female Ossabaw Swine Fed Excess Atherogenic Diet. Comp Med. 2006;56(1).
7. Greenberg AS, Obin MS. Obesity and the role of adipose tissue in inflammation and metabolism2–3.
8. Ibrahim MM. Subcutaneous and visceral adipose tissue: structural and functional differences. Obes Rev. 2010;11(1):11–8.
9. Bechmann LP, Hannivoort RA, Gerken G, Hotamisligil GS, Trauner M, Canbay A. The interaction of hepatic lipid and glucose metabolism in liver diseases. J Hepatol. 2012;56(4):952–64.
10. Lopaschuk GD, Folmes CDL, Stanley WC. Cardiac Energy Metabolism in Obesity. Circul Res. 2007;101(4):335–47.
11. Wang Z, Gerstein M, Snyder M. RNA-Seq: a revolutionary tool for transcriptomics. Nat Rev Genet. 2009;10(1):57–63.
12. Padilla J, Jenkins NT, Lee S, Zhang H, Cui J, Zuidema MY, et al. Vascular transcriptional alterations produced by juvenile obesity in Ossabaw swine. Physiol Genom. 2013 June;45(11):434–46.
13. Toedebusch RG, Roberts MD, Wells KD, Company JM, Kanosky KM, Padilla J, et al. Unique transcriptomic signature of omental adipose tissue in Ossabaw swine: a model of childhood obesity. Physiol Genom. 2014;46(10):362–75.
14. Sassoon DJ, Goodwill AG, Noblet JN, Conteh AM, Herring BP, McClintick JN, et al. Obesity alters molecular and functional cardiac responses to ischemia/reperfusion and glucagon-like peptide-1 receptor agonism. Basic Res Cardiol. 2016;111(4):43.

15. Cai Z, Yu C, Fu D, Pan Y, Huang J, Rong Y et al. Differential metabolic and hepatic transcriptome responses of two miniature pig breeds to high dietary cholesterol. Life Sci. 2020 June 1;250:117514.
16. Qi W, Zhu S, Feng L, Liang J, Guo X, Cheng F, et al. Integrated Analysis of the Transcriptome and Microbial Diversity in the Intestine of Miniature Pig Obesity Model. Microorganisms. 2024;12(2):369.
17. Kleemann R, van Erk M, Verschuren L, Hoek AM, van den, Koek M, Wielinga PY, et al. Time-Resolved and Tissue-Specific Systems Analysis of the Pathogenesis of Insulin Resistance. PLoS ONE. 2010;5(1):e8817.
18. Lützhøft DO, Bækgård C, Wimborne E, Straarup EM, Pedersen KM, Swann JR, et al. High fat diet is associated with gut microbiota dysbiosis and decreased gut microbial derived metabolites related to metabolic health in young Göttingen Minipigs. PLoS ONE. 2024;19(3):e0298602.
19. Swindle MM, Smith AC, editors. Ossabaw Island Miniature Swine: Metabolic Syndrome and Cardiovascular Assessment. In: Swine in the Laboratory [Internet]. 0 ed. CRC Press; 2015 [cited 2025 July 3]. pp. 466–79. Available from: https://www.taylorfrancis.com/books/9781466553521/chapters/10.1201/b19430-22
20. Collection. storage and shipment of specimens for laboratory diagnosis and interpretation of results. In: Surveillance Guidelines for Measles, Rubella and Congenital Rubella Syndrome in the WHO European Region [Internet]. World Health Organization; 2012 [cited 2025 Feb 7]. Available from: https://www.ncbi.nlm.nih.gov/books/NBK143256/
21. Neeb ZP, Edwards JM, Alloosh M, Long X, Mokelke EA, Sturek M. Metabolic Syndrome and Coronary Artery Disease in Ossabaw Compared with Yucatan Swine. Comp Med. 2010;60(4):300–15.
22. Swindle MM, Makin A, Herron AJ, ClubbJr FJ, Frazier KS. Swine as Models in Biomedical Research and Toxicology Testing. Vet Pathol. 2012;49(2):344–56.
23. Sieckmann K, Winnerling N, Huebecker M, Leyendecker P, Juliana Silva Ribeiro D, Gnad T, et al. AdipoQ—a simple, open-source software to quantify adipocyte morphology and function in tissues and in vitro. MBoC. 2022;33(12):br22.
24. Larsen MO, Rolin B. Use of the Göttingen Minipig as a Model of Diabetes, with Special Focus on Type 1 Diabetes Research. ILAR J. 2004;45(3):303–13.
25. Heegaard PMH, Pedersen HG, Jensen AL, Boas U. A robust quantitative solid phase immunoassay for the acute phase protein C-reactive protein (CRP) based on cytidine 5'-diphosphocholine coupled dendrimers. J Immunol Methods. 2009;343(2):112–8.
26. Cirera S. Highly efficient method for isolation of total RNA from adipose tissue. BMC Res Notes. 2013;6(1):472.
27. Chen Y, Chen Y, Shi C, Huang Z, Zhang Y, Li S, et al. SOAPnuke: a MapReduce acceleration-supported software for integrated quality control and preprocessing of high-throughput sequencing data. Gigascience. 2017;7(1):gix120.
28. Ewels P, Magnusson M, Lundin S, Käller M. MultiQC: summarize analysis results for multiple tools and samples in a single report. Bioinformatics. 2016;32(19):3047–8.

29. Patro R, Duggal G, Love MI, Irizarry RA, Kingsford C. Salmon provides fast and bias-aware quantification of transcript expression. Nat Methods. 2017;14(4):417–9.
30. Baldoni PL, Chen Y, Hediyeh-zadeh S, Liao Y, Dong X, Ritchie ME, et al. Dividing out quantification uncertainty allows efficient assessment of differential transcript expression with edgeR. Nucleic Acids Res. 2024;52(3):e13.
31. Ritchie ME, Phipson B, Wu D, Hu Y, Law CW, Shi W, et al. limma powers differential expression analyses for RNA-sequencing and microarray studies. Nucleic Acids Res. 2015;43(7):e47.
32. Gu Z. Complex heatmap visualization. iMeta. 2022 Sept;1(3):e43.
33. Yu G, Wang LG, Han Y, He QY. clusterProfiler: an R Package for Comparing Biological Themes Among Gene Clusters. OMICS. 2012;16(5):284–7.
34. Durinck S, Spellman PT, Birney E, Huber W. Mapping identifiers for the integration of genomic datasets with the R/Bioconductor package biomaRt. Nat Protoc. 2009;4(8):1184–91.
35. Binns D, Dimmer E, Huntley R, Barrell D, O'Donovan C, Apweiler R. QuickGO: a web-based tool for Gene Ontology searching. Bioinformatics. 2009;25(22):3045–6.
36. Evaluation of clustering algorithms for. protein-protein interaction networks | BMC Bioinformatics | Full Text [Internet]. [cited 2025 June 22]. Available from: https://bmcbioinformatics.biomedcentral.com/articles/10.1186/1471-2105-7-488
37. Chin CH, Chen SH, Wu HH, Ho CW, Ko MT, Lin CY. cytoHubba: identifying hub objects and sub-networks from complex interactome. BMC Syst Biol. 2014;8(4):S11.
38. Jensen-Urstad APL, Semenkovich CF. Fatty acid synthase and liver triglyceride metabolism: Housekeeper or messenger? Biochimica et Biophysica Acta (BBA) - Molecular and Cell Biology of Lipids. 2012;1821(5):747–53.
39. Flowers MT, Ntambi JM. Role of stearoyl-coenzyme A desaturase in regulating lipid metabolism. Curr Opin Lipidol 2008 June;19(3):248–56.
40. Guillou H, Zadravec D, Martin PGP, Jacobsson A. The key roles of elongases and desaturases in mammalian fatty acid metabolism: Insights from transgenic mice. Prog Lipid Res. 2010;49(2):186–99.
41. Curtasu MV, Skou Hedemann M, Nygaard Lærke H, Bach Knudsen KE. Obesity Development and Signs of Metabolic Abnormalities in Young Göttingen Minipigs Consuming Energy Dense Diets Varying in Carbohydrate Quality. Nutrients. 2021;13(5):1560.
42. Blüher M. Metabolically Healthy Obesity. Endocrine Reviews. 2020 June 1;41(3):bnaa004.
43. Sturek M, Alloosh M, Sellke FW. Swine Disease Models for Optimal Vascular Engineering. Annu Rev Biomed Eng 2020 June 4;22(1):25–49.
44. Li ZL, Woollard JR, Ebrahimi B, Crane JA, Jordan KL, Lerman A, et al. Transition From Obesity to Metabolic Syndrome Is Associated With Altered Myocardial Autophagy and Apoptosis. ATVB. 2012;32(5):1132–41.

45. Sham JG, Simianu VV, Wright AS, Stewart SD, Alloosh M, Sturek M, et al. Evaluating the Mechanisms of Improved Glucose Homeostasis after Bariatric Surgery in Ossabaw Miniature Swine. J Diabetes Res. 2014;2014(1):526972.
46. Aronson D, Bartha P, Zinder O, Kerner A, Markiewicz W, Avizohar O, et al. Obesity is the major determinant of elevated C-reactive protein in subjects with the metabolic syndrome. Int J Obes. 2004;28(5):674–9.
47. Lee L, Alloosh M, Saxena R, Van Alstine W, Watkins BA, Klaunig JE, et al. Nutritional Model of Steatohepatitis and Metabolic Syndrome in the Ossabaw Miniature Swine. Hepatology. 2009 July;50(1):56–67.
48. Spurlock ME, Gabler NK. The Development of Porcine Models of Obesity and the Metabolic Syndrome1,2. J Nutr. 2008;138(2):397–402.
49. Dahlman I, Forsgren M, Sjögren A, Nordström EA, Kaaman M, Näslund E et al. Downregulation of Electron Transport Chain Genes in Visceral Adipose Tissue in Type 2 Diabetes Independent of Obesity and Possibly Involving Tumor Necrosis Factor-α. Diabetes. 2006 June 1;55(6):1792–9.
50. Ortega FJ, Mayas D, Moreno-Navarrete JM, Catalán V, Gómez-Ambrosi J, Esteve E, et al. The Gene Expression of the Main Lipogenic Enzymes is Downregulated in Visceral Adipose Tissue of Obese Subjects. Obesity. 2010;18(1):13–20.
51. Bergen WG, Mersmann HJ. Comparative Aspects of Lipid Metabolism: Impact on Contemporary Research and Use of Animal Models1. J Nutr. 2005;135(11):2499–502.
52. Li Q, Spalding KL. The regulation of adipocyte growth in white adipose tissue. Front Cell Dev Biol. 2022;10:1003219.
53. Polakof S, Rémond D, Bernalier-Donadille A, Rambeau M, Pujos-Guillot E, Comte B, et al. Metabolic adaptations to HFHS overfeeding: how whole body and tissues postprandial metabolic flexibility adapt in Yucatan mini-pigs. Eur J Nutr. 2018;57(1):119–35.
54. Miyazaki M, Dobrzyn A, Man WC, Chu K, Sampath H, Kim HJ et al. Stearoyl-CoA Desaturase 1 Gene Expression Is Necessary for Fructose-mediated Induction of Lipogenic Gene Expression by Sterol Regulatory Element-binding Protein-1c-dependent and -independent Mechanisms *. Journal of Biological Chemistry. 2004 June 11;279(24):25164–71.
55. Eissing L, Scherer T, Tödter K, Knippschild U, Greve JW, Buurman WA, et al. De novo lipogenesis in human fat and liver is linked to ChREBP-β and metabolic health. Nat Commun. 2013;4(1):1528.
56. Paczkowska-Abdulsalam M, Niemira M, Bielska A, Szałkowska A, Raczkowska BA, Junttila S, et al. Evaluation of Transcriptomic Regulations behind Metabolic Syndrome in Obese and Lean Subjects. Int J Mol Sci. 2020;21(4):1455.
57. Koliaki C, Roden M. Hepatic energy metabolism in human diabetes mellitus, obesity and non-alcoholic fatty liver disease. Mol Cell Endocrinol. 2013;379(1):35–42.
58. Zhao J, Tao C, Chen C, Wang Y, Liu T. Formation of thermogenic adipocytes: What we have learned from pigs. Fundamental Res. 2021 July;1(4):495–502.

59. Zhao JY, Zhou LJ, Ma KL, Rui Hao, Li M. MHO or MUO? White adipose tissue remodeling. Obes Rev. 2024;25(4):e13691.
60. Chattopadhyay M, Guhathakurta I, Behera P, Ranjan KR, Khanna M, Mukhopadhyay S, et al. Mitochondrial bioenergetics is not impaired in nonobese subjects with type 2 diabetes mellitus. Metabolism. 2011;60(12):1702–10.
61. Yin X, Lanza IR, Swain JM, Sarr MG, Nair KS, Jensen MD. Adipocyte Mitochondrial Function Is Reduced in Human Obesity Independent of Fat Cell Size. J Clin Endocrinol Metab. 2014;99(2):E209–16.
62. Ghosh S, Dent R, Harper ME, Gorman SA, Stuart JS, McPherson R. Gene expression profiling in whole blood identifies distinct biological pathways associated with obesity. BMC Med Genom. 2010;3(1):56.
63. Fitzpatrick M, Solberg Woods LC. Adenylate cyclase 3: a potential genetic link between obesity and major depressive disorder. Physiol Genom. 2024;56(1):1–8.
64. Zhong J, Zareifi D, Weinbrenner S, Hansen M, Klingelhuber F, Nono Nankam PA, et al. adiposetissue.org: A knowledge portal integrating clinical and experimental data from human adipose tissue. Cell Metabol. 2025;37(3):566–9.
65. AT Knowledge Portal [Internet]. [cited 2025 July 23]. Available from: https://adiposetissue.org/
66. Alligier M, Meugnier E, Debard C, Lambert-Porcheron S, Chanseaume E, Sothier M, et al. Subcutaneous Adipose Tissue Remodeling during the Initial Phase of Weight Gain Induced by Overfeeding in Humans. J Clin Endocrinol Metab. 2012;97(2):E183–92.
67. Kagan HM. Lysyl Oxidase: Mechanism, Regulation and Relationship to Liver Fibrosis. Pathol - Res Pract. 1994;190(9):910–9.
68. Li C, Li,Jing, He, Fang, Li, Kun, Li, Xu, and, Zhang Y. Matrix Gla protein regulates adipogenesis and is serum marker of visceral adiposity. Adipocyte. 2020;9(1):68–76.
69. Sánchez-Ceinos J, Guzmán-Ruiz R, Rangel-Zúñiga OA, López-Alcalá J, Moreno-Caño E, Del Río-Moreno M et al. Impaired mRNA splicing and proteostasis in preadipocytes in obesity-related metabolic disease. eLife. 2021 Sept 21;10:e65996.
70. Başarır Sivri FN, Çiftçi S. A New Insight into Fatty Acid Binding Protein 4 Mechanisms and Therapeutic Implications in Obesity-Associated Diseases: A Mini Review. Mol Nutr Food Res. 2024;68(8):2300840.
71. Stahl A, Evans JG, Pattel S, Hirsch D, Lodish HF. Insulin Causes Fatty Acid Transport Protein Translocation and Enhanced Fatty Acid Uptake in Adipocytes. Dev Cell. 2002;2(4):477–88.
72. Huang J, Zhu R, Shi D. The role of FATP1 in lipid accumulation: a review. Mol Cell Biochem. 2021;476(4):1897–903.
73. Wu Q, Ortegon AM, Tsang B, Doege H, Feingold KR, Stahl A. FATP1 Is an Insulin-Sensitive Fatty Acid Transporter Involved in Diet-Induced Obesity. Mol Cell Biol. 2006;26(9):3455–67.

74. Skurk T, Alberti-Huber C, Herder C, Hauner H. Relationship between Adipocyte Size and Adipokine Expression and Secretion. J Clin Endocrinol Metabolism. 2007;92(3):1023–33.
75. Pauter AM, Olsson P, Asadi A, Herslöf B, Csikasz RI, Zadravec D, et al. Elovl2 ablation demonstrates that systemic DHA is endogenously produced and is essential for lipid homeostasis in mice. J Lipid Res. 2014;55(4):718–28.
76. Li X, Liu C, Zhang R, Li Y, Ye D, Wang H et al. Biosynthetic deficiency of docosahexaenoic acid causes nonalcoholic fatty liver disease and ferroptosis-mediated hepatocyte injury. Journal of Biological Chemistry. 2024 July 1;300(7):107405.
77. Yu JE, Han SY, Wolfson B, Zhou Q. The Role of Endothelial Lipase in Lipid Metabolism, Inflammation, and Cancer. Histol Histopathol. 2018;33(1):1–10.
78. Torres N, Tobón-Cornejo S, Velazquez-Villegas LA, Noriega LG, Alemán-Escondrillas G, Tovar AR. Amino Acid Catabolism: An Overlooked Area of Metabolism. Nutrients. 2023;15(15):3378.
79. Moon J, Do HJ, Cho Y, Shin MJ. Arginase Inhibition Ameliorates Hepatic Metabolic Abnormalities in Obese Mice. PLoS ONE. 2014 July;24(7):e103048.
80. Liao Y, Chen Q, Liu L, Huang H, Sun J, Bai X, et al. Amino acid is a major carbon source for hepatic lipogenesis. Cell Metabol. 2024;36(11):2437–e24488.
81. Bruinstroop E, Zhou J, Tripathi M, Yau WW, Boelen A, Singh BK et al. Early induction of hepatic deiodinase type 1 inhibits hepatosteatosis during NAFLD progression. Mol Metab 2021 June 5;53:101266.

Figures

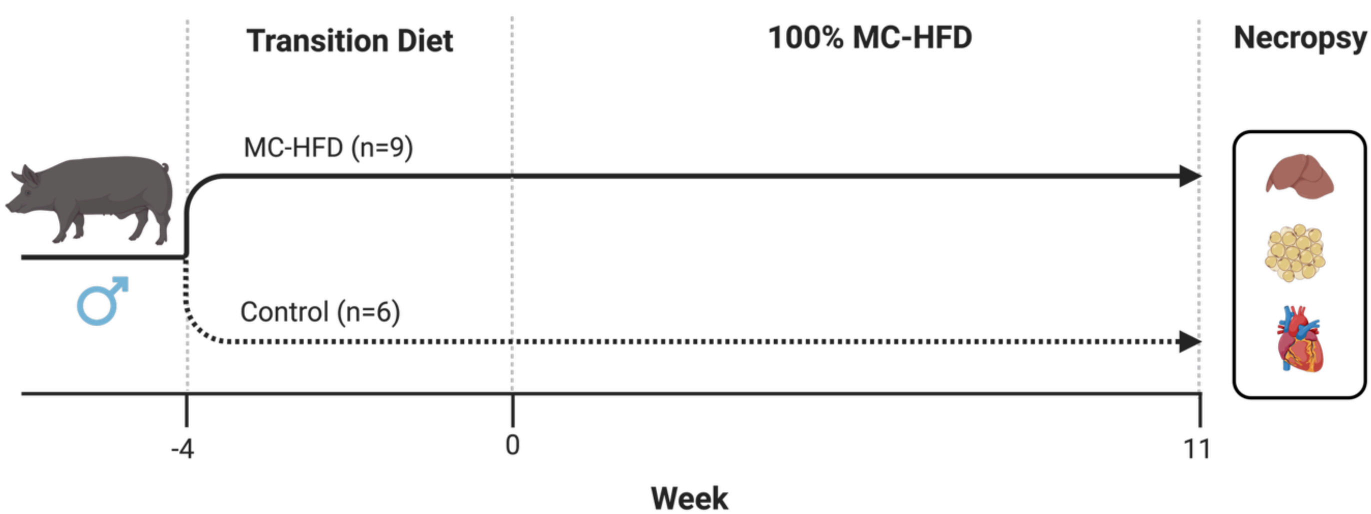

Figure 1

Experimental setup. Male, castrated miniature Ossabaw pigs randomized into two groups: a control group fed a chow diet, and a group fed a medium cholesterol, high-fat, high-fructose diet (MC-HFD) for 11 weeks. A transition period was implemented to gradually adjust the MC-HFD pigs to the fat feed. BW and ABC were measured, and blood samples were collected from all animals throughout the study. At necropsy, tissues sampled included liver, heart, VAT and SAT. Created using Biorender.com

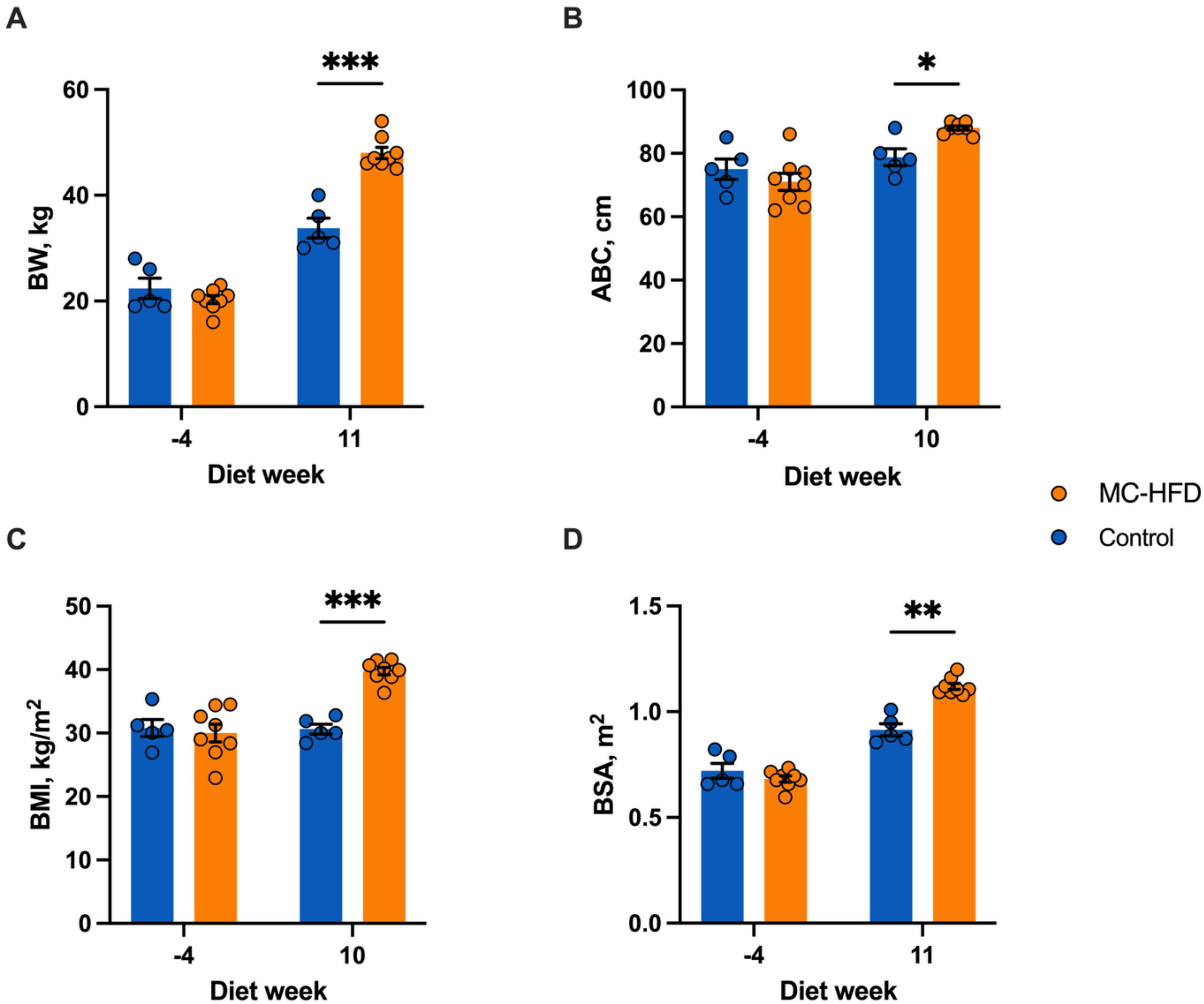

Figure 2

Morphometric parameters measured at the start and end of the study. Statistical significance between control (n=5) and MC-HFD (N=8) group at individual time points was determined with unpaired Welch´s t-test and Holm-Šídák corrections (*P < 0.05, **P < 0.01, ***P < 0.001). Error bars depict standard error of the mean (SEM). Circumference measurements were not taken at week 11, therefore, week 10 were used instead. BW: body weight. ABC: abdominal circumference. BMI: body mass index. BSA: body surface area.

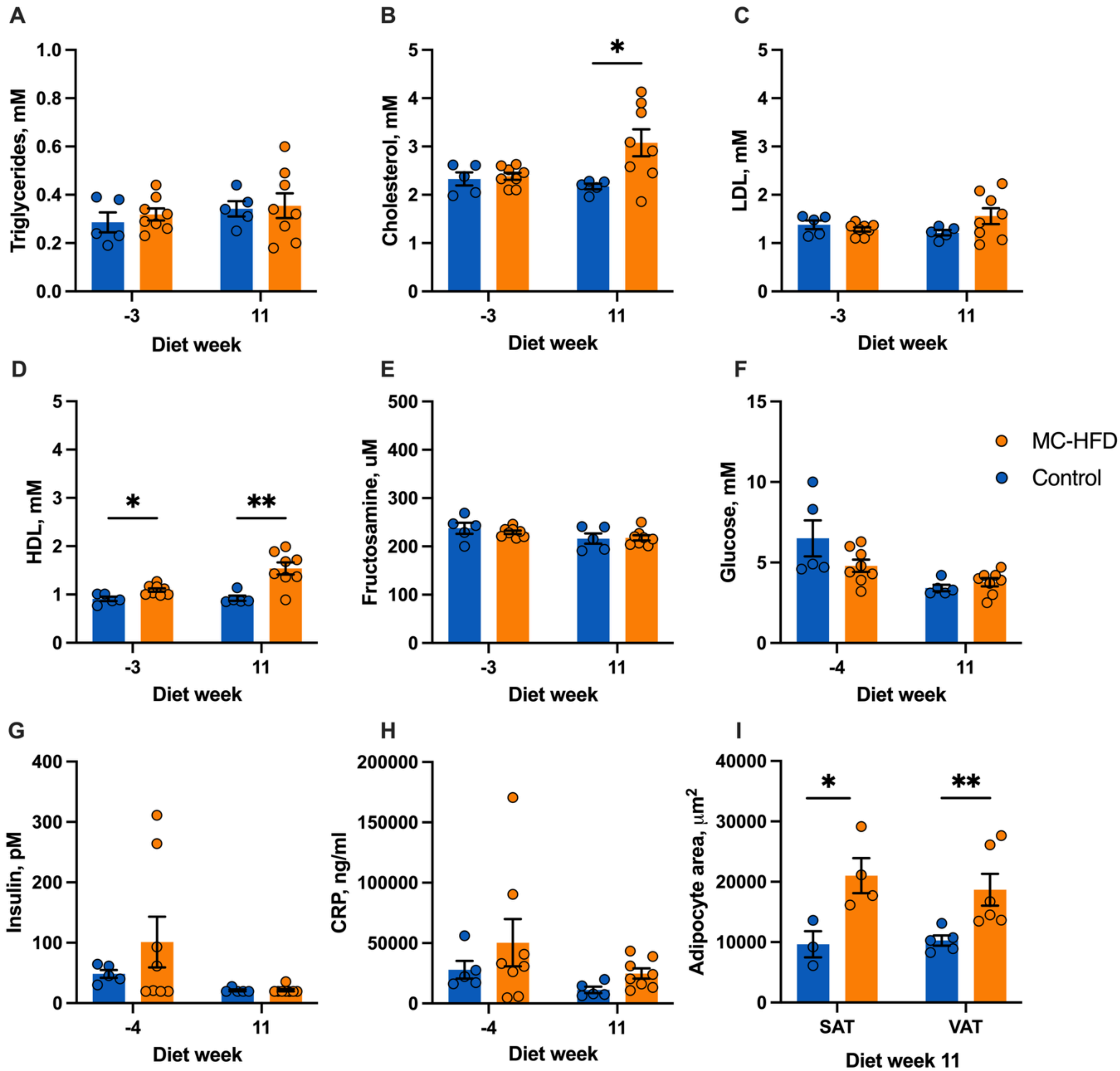

Figure 3

Blood biomarkers of MetS and inflammation measured in fasting serum samples from the start and end of the study, and adipocyte area of VAT and SAT sampled at necropsy. Statistical significance between control (n=5) and MC-HFD (n=8) group at individual time points was evaluated with unpaired Welch´s t-test, for normally distributed data, and Holm-Šídák corrections. For not normally distributed data a non-parametric alternative (Mann-Whitney test) was used (*P < 0.05, **P < 0.01). To test group differences in average adipocyte area, an unpaired two-tailed Welch´s t-test was performed for SAT dataset, while the non-parametric test was used for VAT dataset. Error bars depict SEM. LDL: low-density lipoprotein. HDL: high-density lipoprotein. CRP: C-reactive protein.

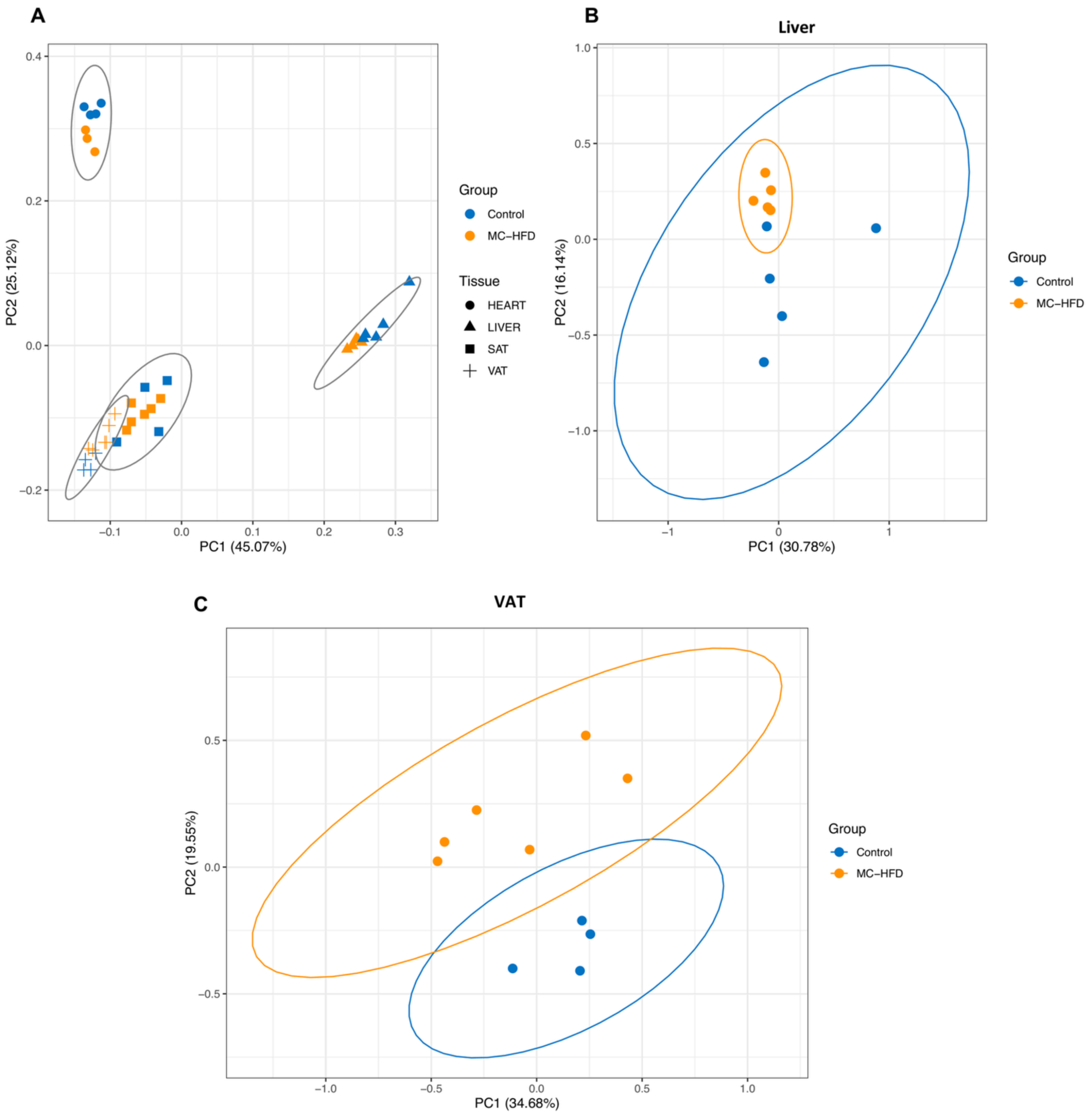

Figure 4

PCA of RNA-seq data. PCA plot of RNA-seq data organized by tissue and group **(A),** from liver **(B)**and AT depots **(C)**. Data points indicate a pig sample. Colour: diet group. In **(A)** tissue type is indicated by circles, in **(B)**and **(C)**, diet groups are encircled. Axes depict PC1-2, including the % of variance explained. RNA-seq data used for PCA was pre-processed by filterByExpr using the default settings, followed by CPM for normalization and log2 transformation. To perform PCA analysis prcomp was used with the default settings. Stat_ellipse was used to compute an ellipse assuming a multivariate normal distribution.

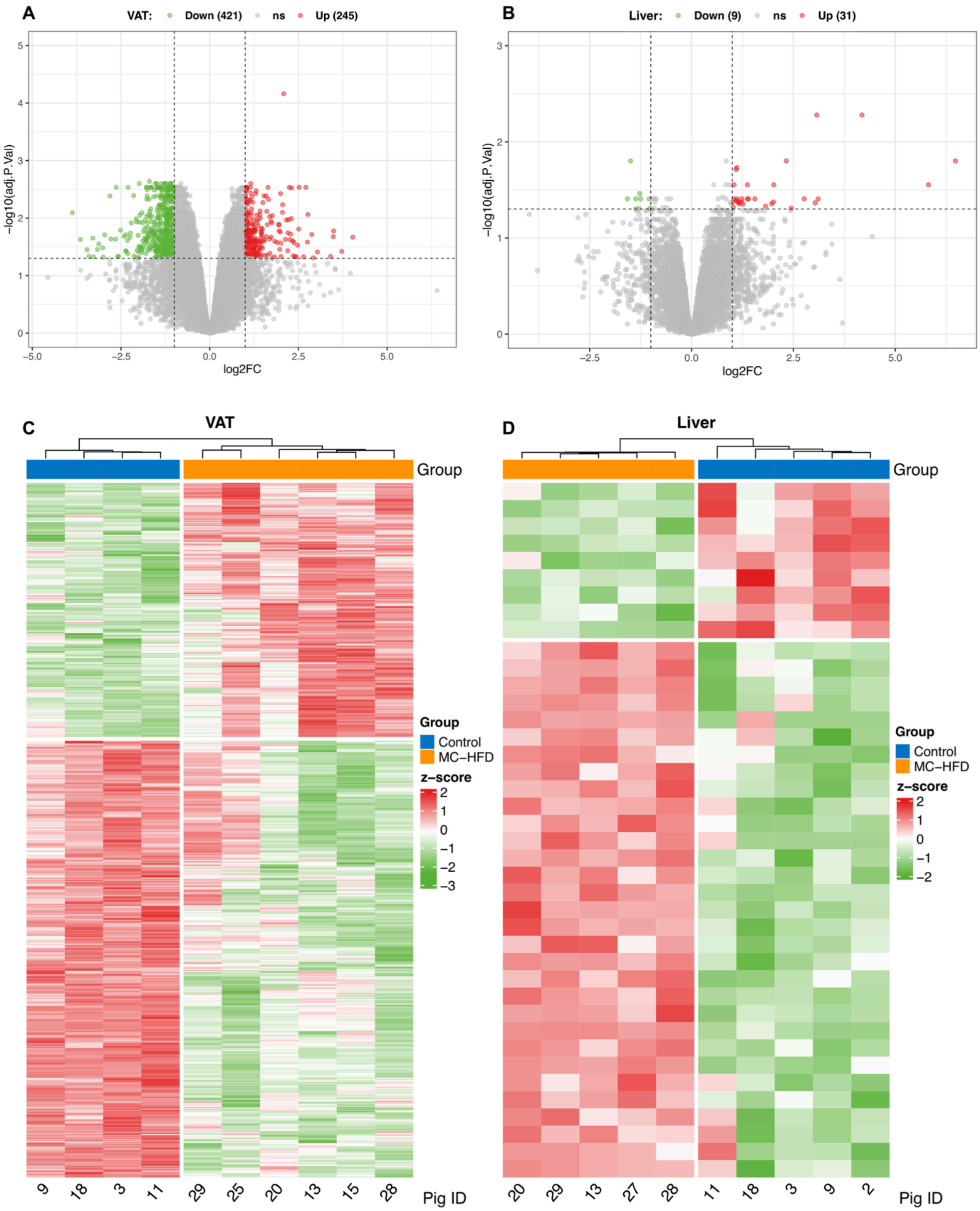

Figure 5

Differential expression analysis of RNA-seq data from VAT and liver. Volcano plot showing DETs in MC-HFD vs. control for **(A)** VAT and **(B)** liver. Statistical significance:êlog$_2$FCï≥ 1 and P.adj < 0.05. Color:

upregulated in red, downregulated in green, non-significant in grey (MC-HFD vs. controls). Two-way hierarchical clustering heatmap of DETs in **(C)** VAT and **(D)** liver. Each column corresponds to a sample and each row to a transcript. Transcript expression values were normalized and log2-transformed. Z-score reflects the scaled expression of each transcript across the samples. Colour: red for higher expression and green for lower expression (MC-HFD vs. controls). Columns are labelled with the corresponding pig identification (Pig ID) at the bottom and colour coded according to diet group at the top.

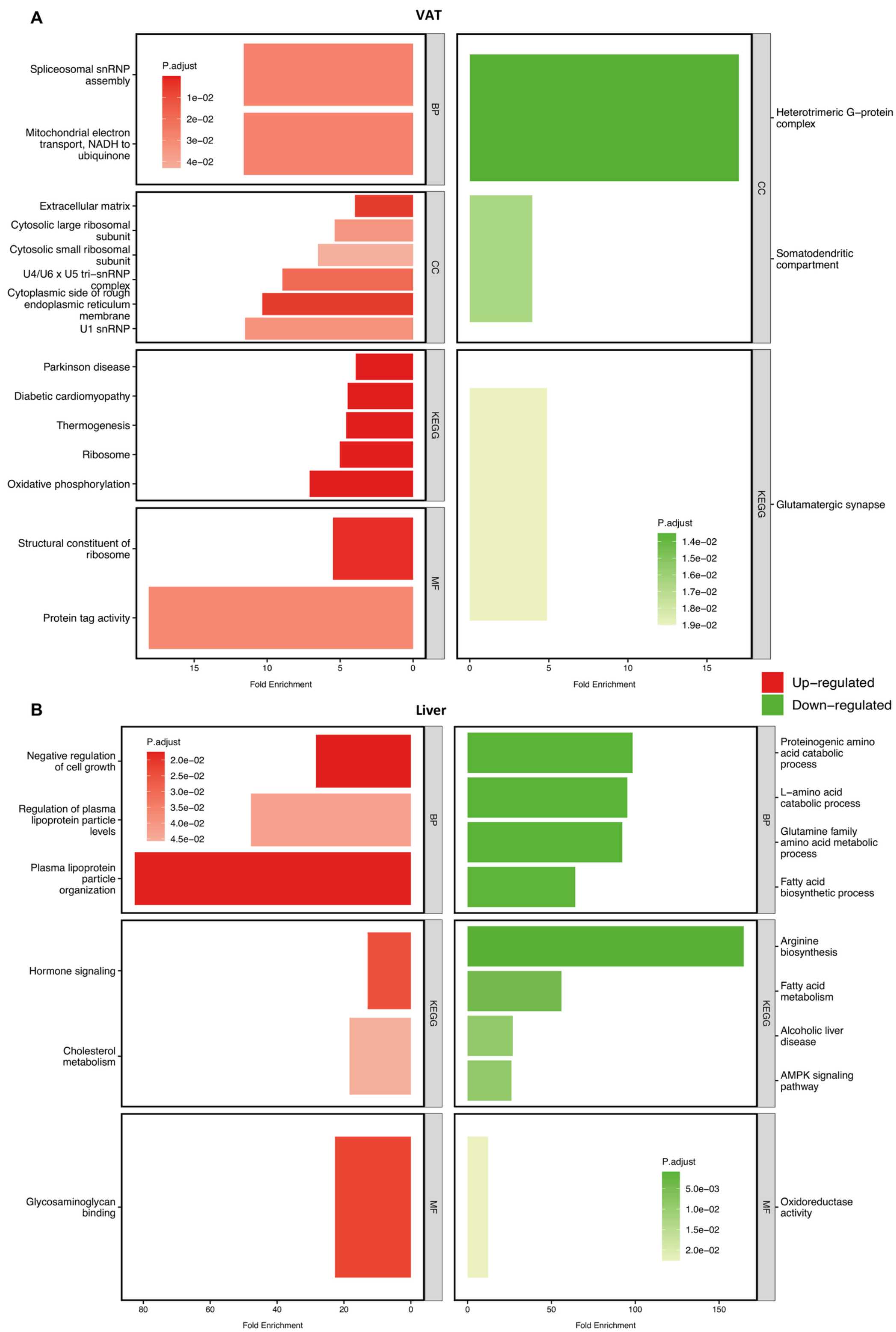

Figure 6

GO and KEGG enrichment analysis of DETs summarized at the gene level. (A) Overrepresentation analysis of DE results in VAT. **(B)** Overrepresentation analysis of DE results in liver. Left panels in red shows overrepresented terms in significantly upregulated genes (MC-HFD vs. control, P.adj < 0.05, $\log_2$FC ≥ 1). Right panels in green show overrepresented terms in significantly downregulated genes (MC-HFD vs. control, P.adj < 0.05, $\log_2$FC ≤ -1). Each separate compartment corresponds to one of the three GO categories (CC, MF or BP) or KEGG. Color gradient: degree of significance by adjusted P-value.

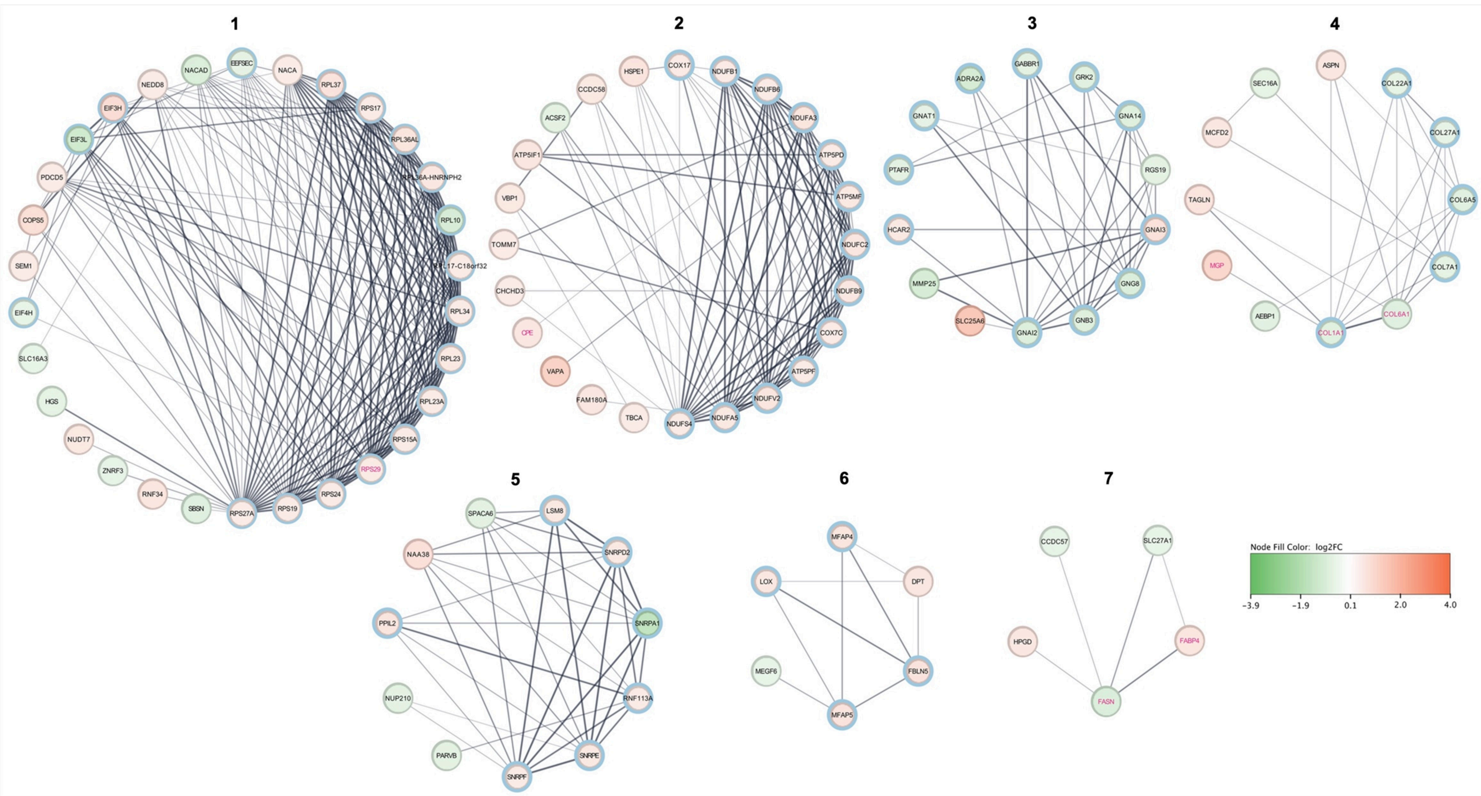

Figure 7

Clusters identified in VAT PPI network. The figure illustrates seven selected functional protein interaction clusters, identified using the Markov Cluster (MCL) algorithm through the clusterMaker2 plugin and visualized with Cytoscape software. Clusters are identified by numbers 1-7. In the network, nodes represent proteins and edges indicate functional or physical protein interactions, with edge thickness indicating the strength of supporting data. Node colors represent log2FC expression changes (MC-HFD vs. control). Pink gene symbols indicate that the node is present at the intersection between DE results and obesity-related genes. Blue border indicates which nodes belong to the GO or KEGG term used to annotate the cluster. All clusters were displayed in a degree-sorted circular layout, where the node with the highest number of interactions (degree) is positioned at 6 o’clock, and the remaining nodes follow counterclockwise in descending order.

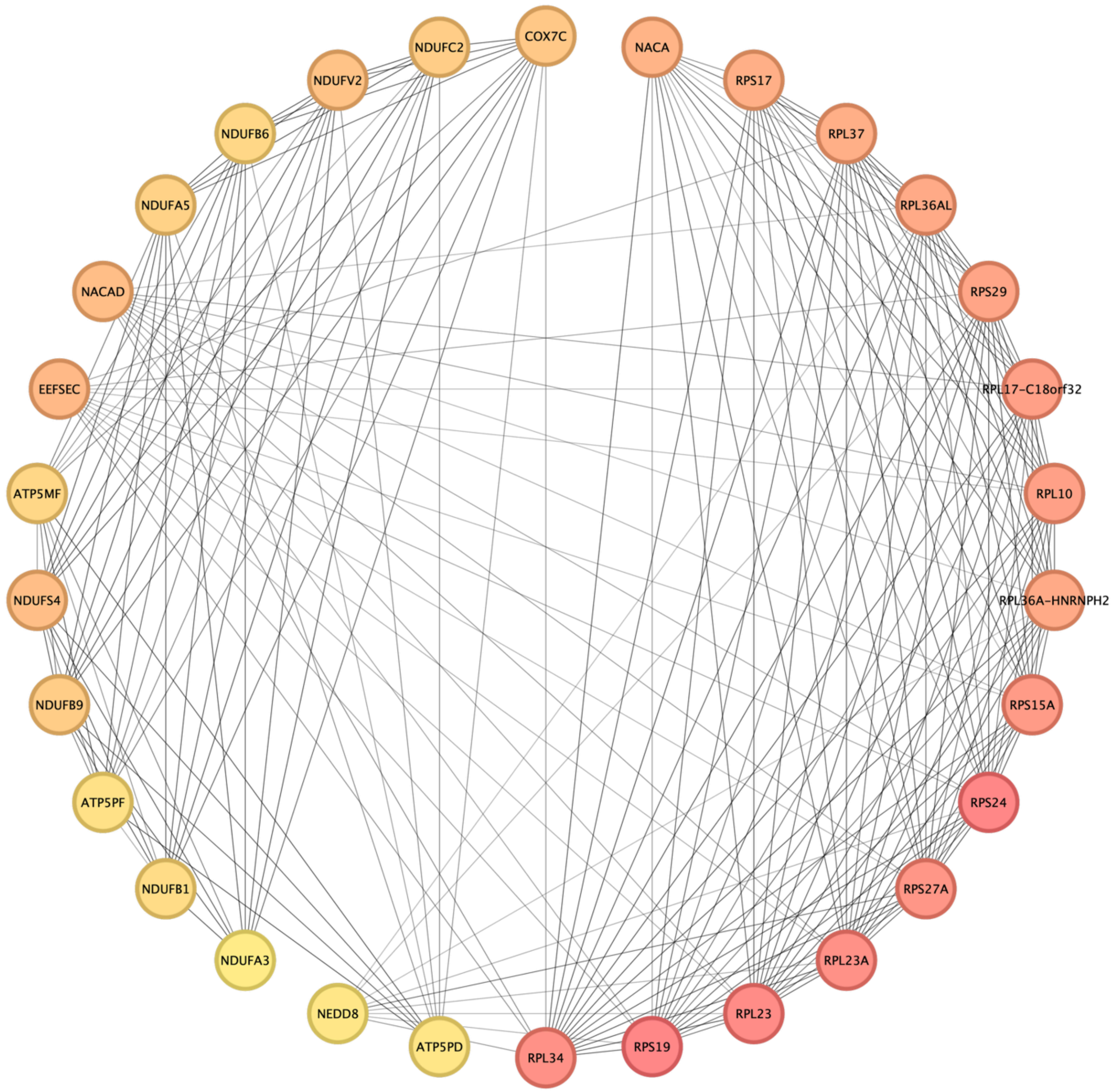

Figure 8

Hub analysis in VAT PPI Network. The top 30 core proteins in the VAT network were identified using the MCC algorithm via the cytoHubba plugin and visualized with Cytoscape software using a degree-sorted circular layout, where the node with the highest number of interactions (degree) is positioned at 6 o'clock, and the remaining nodes are arranged counterclockwise in descending order of interactions (degree value). Nodes represent proteins and edges indicate functional or physical protein interactions. Node colors follow a gradient based on the MCC score, ranging from yellow (lowest) to red (highest).

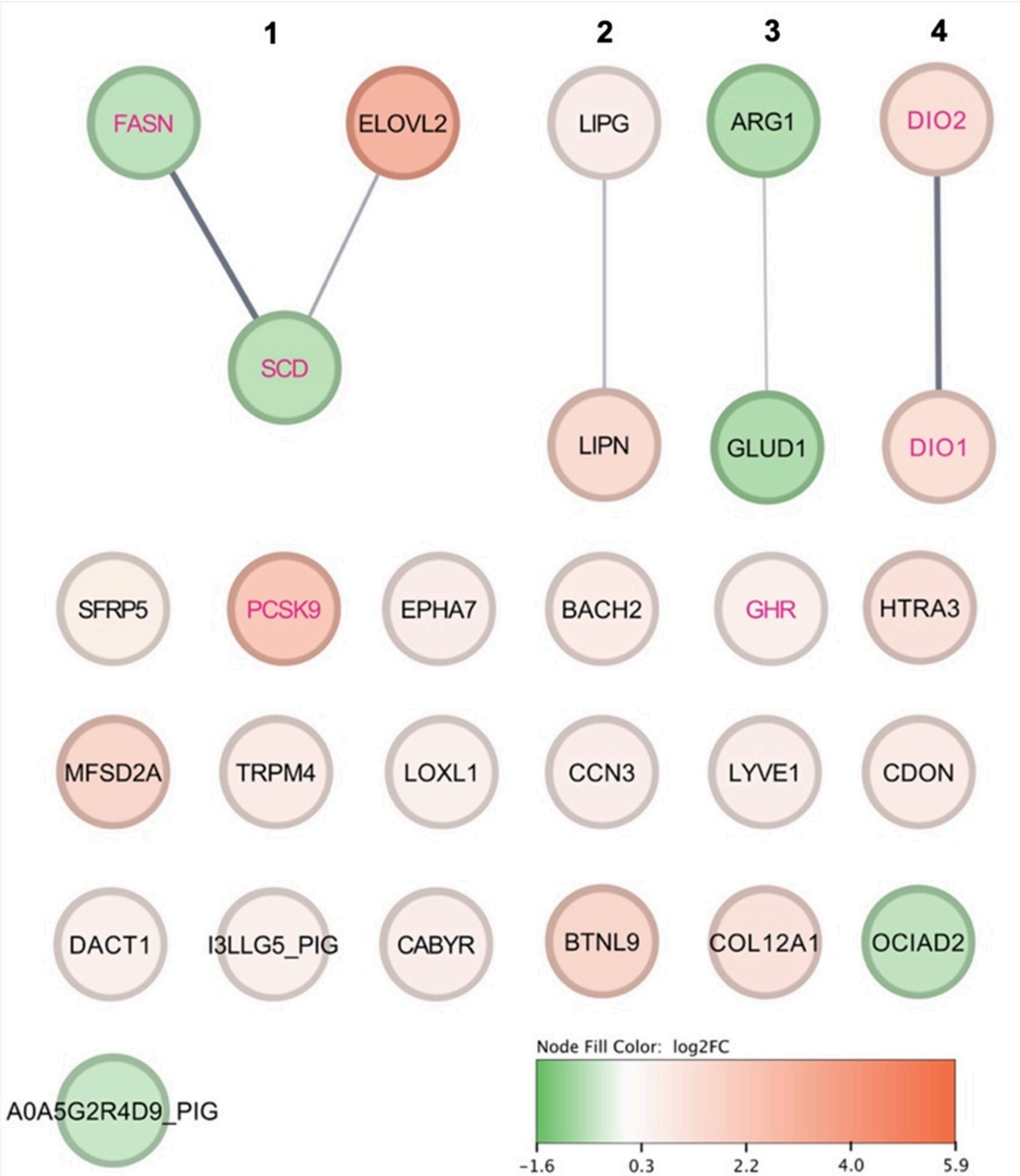

Figure 9

PPI network of liver DETs summarized at the gene level. Network was constructed using STRING database and visualized through Cytoscape software. Nodes represent proteins and edges indicate functional or physical protein interactions, with edge thickness indicating the strength of supporting data. Node colors represent log2FC expression changes (MC-HFD vs. control). A threshold of 0.4 was chosen for the edge confidence. The network includes 28 nodes and 5 edges, with a significant number of interactions observed (P = 0.0131). Subnetworks are identified by numbers 1-4. Pink gene symbols indicate that the node is present at the intersection with obesity-related genes.

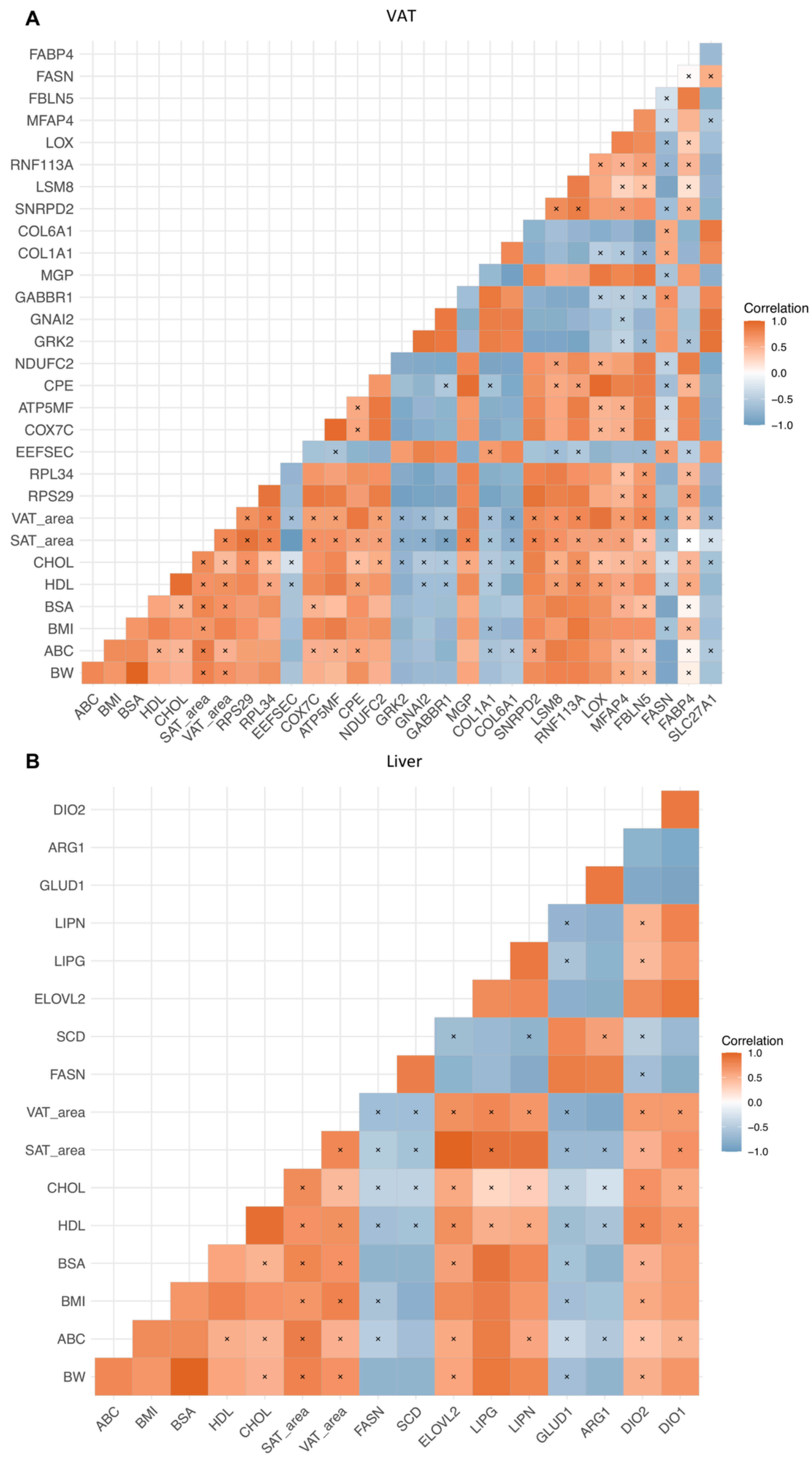

Figure 10

Correlation between gene expression and phenotypic traits. The heatmap shows Spearman correlation between the expression of the selected genes (normalized and $\log_2$-transformed) and phenotypic parameters that differed significantly between diet groups. Blue squares indicate negative correlation coefficients and orange squares positive ones. ‘x’ indicates a non-significant correlation after Benjamini-Hochberg (BH) correction. In case of missing values, the association is computed based on pairwise completeness for each variable pair. **(A)** Correlation with VAT selected genes. **(B)** Correlation with liver selected genes. CHOL, cholesterol.

Supplementary Files

This is a list of supplementary files associated with this preprint. Click to download.

- Supplementarydata.docx
- Supplementaryfile2.xlsx
- Supplementaryfile3.xlsx
- supplementaryfile9.xlsx
- supplementaryfile5.xlsx
- supplementaryfile8.xlsx
- Supplmentaryfile1.xlsx
- supplementaryfile6.xlsx
- Supplementaryfile4.xlsx
- supplementaryfile7.xlsx